AD-A180 013 TEMPERATURE FIELD IN THE VICINITY OF A NEAR-SURFACE VOID DUE TO HIGH-SPEE (U) NEW MEXICO UNIV ALBUQUERQUE DEPT OF MECHANICAL ENGINEERING F D JU ET AL FEB 87 1/1

UNCLASSIFIED ME-140(86)ONR-233-3 N00014-84-K-0252 F/G 20/13 NL

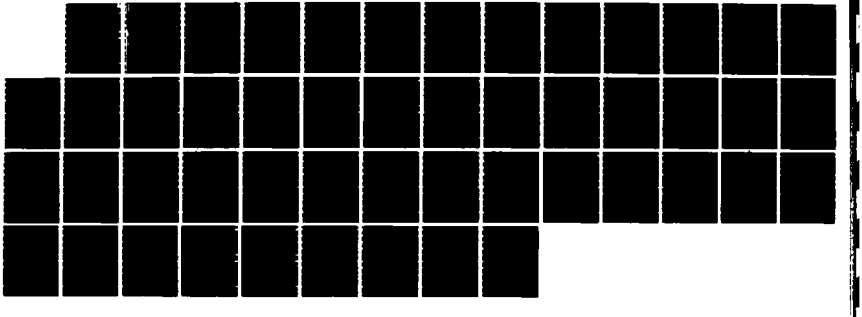

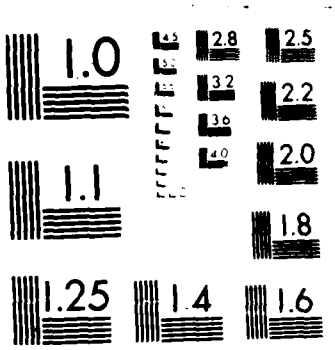

THE UNIVERSITY OF NEW MEXICO
COLLEGE OF ENGINEERING

BUREAU OF ENGINEERING RESEARCH

Temperature Field in the Vicinity of a Near-Surface Void Due to High-Speed Friction Load

by
Frederick D. Ju and Tsu-Yen Chen
The University of New Mexico

Technical Report
ME-140(86)ONR-233-3

Work Performed Under Contract No. ONR-N00014-84-K-0252

February 1987

Technical Report

Temperature Field in the Vicinity of a Near-Surface Void Due to High-Speed Friction Load

by

Frederick D. Ju
Presidential Professor

and

Tsu-Yen Chen
Research Assistant

Mechanical Engineering Department

University of New Mexico

Albuquerque, New Mexico 87131

February 1987

ACKNOWLEDGEMENT

The present research is performed under a grant from the Office of Naval Research, Grant No. N00014-84-K-0252. Dr. Peter J. Blau is the program manager.

ABSTRACT

The present investigation expounds on the effect of a near-surface cavity, when the solid surface is subjected to the Coulomb frictional loading of an asperity moving at moderately high-speed. The medium under consideration is represented by a solid half space which is coated with a thin layer of solid wear coating. The cavity in the present report is rectangular. The temperature field and its gradient in the vicinity of the cavity result from the traverse of the asperity over the wear surface near the cavity. The cavity defect results in a material nonuniformity mathematically modelled in terms of the material coordinates. The resulting governing differential equation is time-explicit and transient. A general finite difference formulation is developed, from which numerical solutions were obtained for problems with a cavity at various positions relative to the surface-layer/substrate interface. Because of the poor heat transfer characteristics of the cavity, the temperatures in the surface layer above it are higher than those in the surrounding region. This phenomenon causes a higher temperature gradient, especially at the trailing corner of the rectangular cavity. There, the direction of the maximum temperature gradient is at a significant oblique angle to the wear surface. The combined effect of a higher temperature gradient and an oblique direction would result in a much larger shear stress in the surface-layer/substrate interface. This phenomenon could lead toward delamination of the coating near the cavity.

TABLE OF CONTENTS

LIST OF FIGURES

Figure

13. Dimensionless heat flux in ξ-direction.

14. Dimensionless heat flux in η-direction.

15. Dimensionless temperature field, showing thermal property effects.

Case 2B, 2C, 2D, 2E - coated material with a cavity, the top edge of the cavity is at the interface, showing thermal property changes in comparison to Case 4.

Case 2B - The material properties of the substrate are the same as the surface layer except that $k_2 = 2k_1$, $\rho c_2 = 2\rho c_1$.

Case 2C - The material properties of the substrate are the same as the surface layer except that $k_2 = 0.5k_1$, $\rho c_2 = 0.5\rho c_1$.

Case 2D - The material properties of the substrate are the same as the surface layer except that $k_2 = k_1$, $\rho c_2 = 0.5\rho c_1$.

Case 2E - The material properties of the substrate are the same as the surface layer except that $k_2 = 2k_1$, $\rho c_2 = \rho c_1$.

Case 4 - single material with a cavity, the material is silicon carbide, $L = 0.04a$.

16. Dimensionless heat flux in ξ-direction; $\eta = 0$.

17. Dimensionless heat flux in ξ-direction, $\eta = 0.04$.

18. Dimensionless temperature field for single material without cavity and coated material with cavity, $L = 0.04a$.

NOMENCLATURE

a	asperity width
b	substrate thickness
C	specific heat
c(t)	distance from x_1 origion to the center of the asperity
D	dimensionless coating thickness (H/a)
d	half width of the cavity
e	depth of the cavity
H	coating thickness
k_1, k_2	thermal conductivity of surface layer and substrate
L	ligament thickness
P(i,j)	center of the finite difference cell
M,N,R,S	surrounding points of P
$P'(x_1,t)$	pressure over the contact area
$q(x_1,t)$	heat flux through the contact area
q_o	average heat flux through the contact area
$Q_{S\rightarrow P}$	heat flux from point S to point P
$Q^*(=q/q_o)$	dimensionless heat flux through the contact area
R_1, R_2	Peclet numbers of surface layer and substrate ($R_i = va/\kappa_i$)
T	temperature
U	internal energy
v	traverse speed of asperity
w	width of the total rectangular finite difference region
w'	distance from x_1 origin to the center of the cavity
ξ	dimensionless coordinate ($=x_1/a$)
η	dimensionless coordinate ($=x_2/a$)

$\bar{\xi}, \bar{\eta}$	coordinates in transformed plane
κ_1, κ_2	thermal diffusivity of surface layer and substrate
μ_f	Coulomb coefficient of friction
α	thermal diffusivity ratio ($\alpha^2 = \kappa_2/\kappa_1$)
β	thermal conductivity ratio ($\beta = k_2/k_1$)
ϕ	dimensionless temperature ($\phi = Tk_1/q_o a$)
ρ	mass density
τ	dimensionless time ($\tau = vt/a$)

CHAPTER I

INTRODUCTION

The present investigation constitutes a portion of the general problem of the thermo-mechanical effect of a moving asperity over a solid medium with a solid coating layer. The asperity, generally on the order of a millimeter, traverses over the solid surface at a uniform moderately-high speed, approximately 15 ms^{-1}, and excites the solid surface mechanically and thermally through Coulomb friction. When there is no flaw in the uniformly coated region, the problem can be formulated with a asperity-fixed coordinate system for steady-state solutions. Ju and Chen [1] first solved for the case of a moderately thick coating. Later Ju and Liu [2] extended the general formulation of [1] to study the thickness effect of the coating layer for various mechanical and thermal impedance mismatching between the surface coating layer and the substrate. In both cases, the results of Huang and Ju [3] were verified that, at such a moderately high speed, the stresses from the thermal effect of the asperity friction are an order of magnitude larger than those from its mechanical traction effect. The present investigation, therefore, will concentrate on the temperature field and the temperature gradient surrounding a flaw in the form of a rectangular cavity. This cavity is located in the surface layer or at the coating-layer/substrate interface.

The physical model of asperity friction was based on the experimental studies in works by Archard [4] and Bannerjee and Burton [5]. Because of the three-dimensional aspect of those observed "hot spots", Huang and Ju [3] formulated the problem in three-dimensional theory of the thermo-mechanical effect owing to the Coulomb friction of moving asperities over a single

solid wear medium. In its application to the problem of a single high speed asperity, it was observed that: (i) at an asperity traversing speed of 10-15 ms^{-1}, the thermal stress as a result of high temperature gradients is eight times the stress due to mechanical loading, (ii) at such asperity speed, the maximum tensile stress is the largest at a depth of about one tenth the asperity size, i.e., at a depth of the order of 100 μm, and (iii) while the surface temperature is the same for the three-dimensional model as compared with that of two-dimensional model [6], the resulting maximum stress is six times higher for the three-dimensional model due to much higher temperature gradient. Therefore, for the thermo-mechanical analysis of the effect of an imbedded flaw, it is primarily important to obtain first a temperature field solution.

In the previous works of the moving asperity problem, the analyses dealt with basically uniform solid medium, that is, the material and asperity properties are invariant in the direction of the asperity motion. In such a case, the time effect can be rendered implicit in the Fourier and Navier equations by using a coordinate system fixed to the asperity (called the convective coordinate system) traversing therewith [1,2,3]. The resulting steady-state solutions are not explicitly time-dependent in such coordinates. When a flaw, such as a cavity, exists in the medium, uniformity in the direction of asperity motion no longer exists. A coordinate system fixed to the cavity, or to the material, (referred to as the material coordinates) must be employed by necessity. As the asperity traverses over the surface under which the cavity lies, the induced temperature field has to be an explicit function of time. The solutions are transient. The steady-state solution of the temperature field resulting from the moving

asperity over an uniform medium has been dealt with by several authors [1,2,3,6,7,8,9,10], whereas the transient solution for a flawed medium is lacking.

CHAPTER II

ANALYTICAL MODEL

While the three-dimensional model gives a more accurate description, it is considered that, for the purpose of studying the effect of a cavity, a two-dimensional model is adequate, with considerably simpler mathematical operation. The general geometry is shown in Figure 1.

2.1 Governing Mathematical Equations

The mathematical model is a semi-infinite body with a thin coating layer and a rectangular cavity in the neighborhood of the coating-layer/substrate interface. The half space surface is subjected to the frictional heating of a moving asperity over the surface.

The governing equations are as follows: In the surface layer, $0 < \eta < D$, denoted by the superscript (1),

$$\frac{\partial^2 \phi^{(1)}}{\partial \xi^2} + \frac{\partial^2 \phi^{(1)}}{\partial \eta^2} = R_1 \frac{\partial \phi^{(1)}}{\partial \tau} . \qquad (1)$$

In the substrate region, $D < \eta < \infty$, denoted by the superscript (2),

$$\frac{\partial^2 \phi^{(2)}}{\partial \xi^2} + \frac{\partial^2 \phi^{(2)}}{\partial \eta^2} = R_2 \frac{\partial \phi^{(2)}}{\partial \tau} , \qquad (2)$$

where $\phi(=Tk_1/q_o a)$ is the dimensionless temperature, $(\xi,\eta)(=x_i/a)$ are the dimensionless coordinates in the direction opposed to the asperity motion, and the depth, direction respectively, $\tau(=vt/a)$ is the dimensionless time, $D = H/a$ the dimensionless coating thickness, $R_i = va/\kappa_i$ the Peclet numbers in the coating layer (i=1) and in the substrate (i=2), and $Q^*(=q/q_o)$ is the dimensionless heat flux from the asperity friction normalized by the average

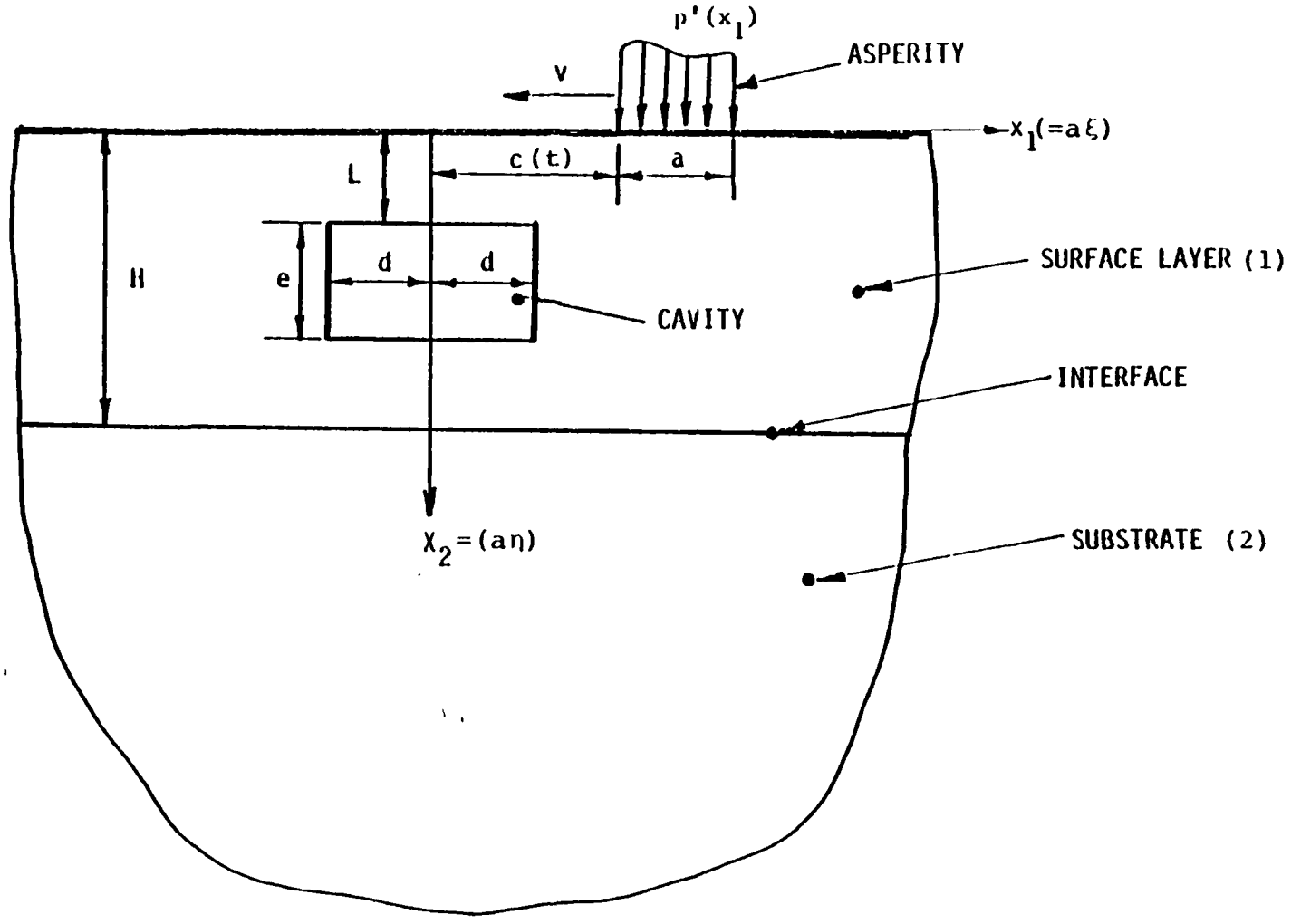

Figure 1. Two dimensional model of coated wear surface with cavity.

heat flux q_o in the contact area, v is the asperity traversing speed, a is the asperity width in the traversing direction, κ_i is the thermal diffusivity in the region (i).

The temperature field ϕ must satisfy the following conditions:

1° the initial condition,

$$\phi^{(i)}(\xi,\eta,0) = 0, \qquad i = 1,2 \tag{3}$$

2° the boundary conditions:

(i) at infinity, $\xi^2 + \eta^2 \to \infty$, the regularity conditions are

$$\phi^{(1)}, \phi^{(2)} = 0,$$

(ii) in the asperity contact surface, $c(\tau)/a \le \xi \le (c(\tau)/a)+1$, $\eta = 0$, the heat input through the boundary is the rate of the frictional energy

$$-\frac{\partial \phi^{(1)}}{\partial \eta} = Q^* = q/q_o,$$

where $q = \mu_f v P'$, $\mu_f P'$ is the asperity friction force in the contact region,

(iii) outside the contact surface, $\xi < c(\tau)/a$ or $\xi > (c(\tau)/a)+1$, $\eta = 0$, without loss of generality, the surface is adiabatic

$$-\frac{\partial \phi^{(1)}}{\partial \eta} = 0 , \tag{5}$$

3° at the layer/substrate interface, $\eta = D$, the continuity conditions for the heat flux must be satisfied.

$$\phi^{(1)} = \phi^{(2)}$$

and

$$\frac{\partial \phi^{(1)}}{\partial \eta} = \beta \frac{\partial \phi^{(2)}}{\partial \eta} , \tag{6}$$

where β $(=k_2/k_1)$ is the thermal conductivity ratio,

4° adiabatic conditions at cavity boundaries,

$$\frac{\partial \phi}{\partial \xi} = 0, \text{ at } \xi = \pm d/a, \; L \le \eta \le (L+e)/a, \tag{7}$$

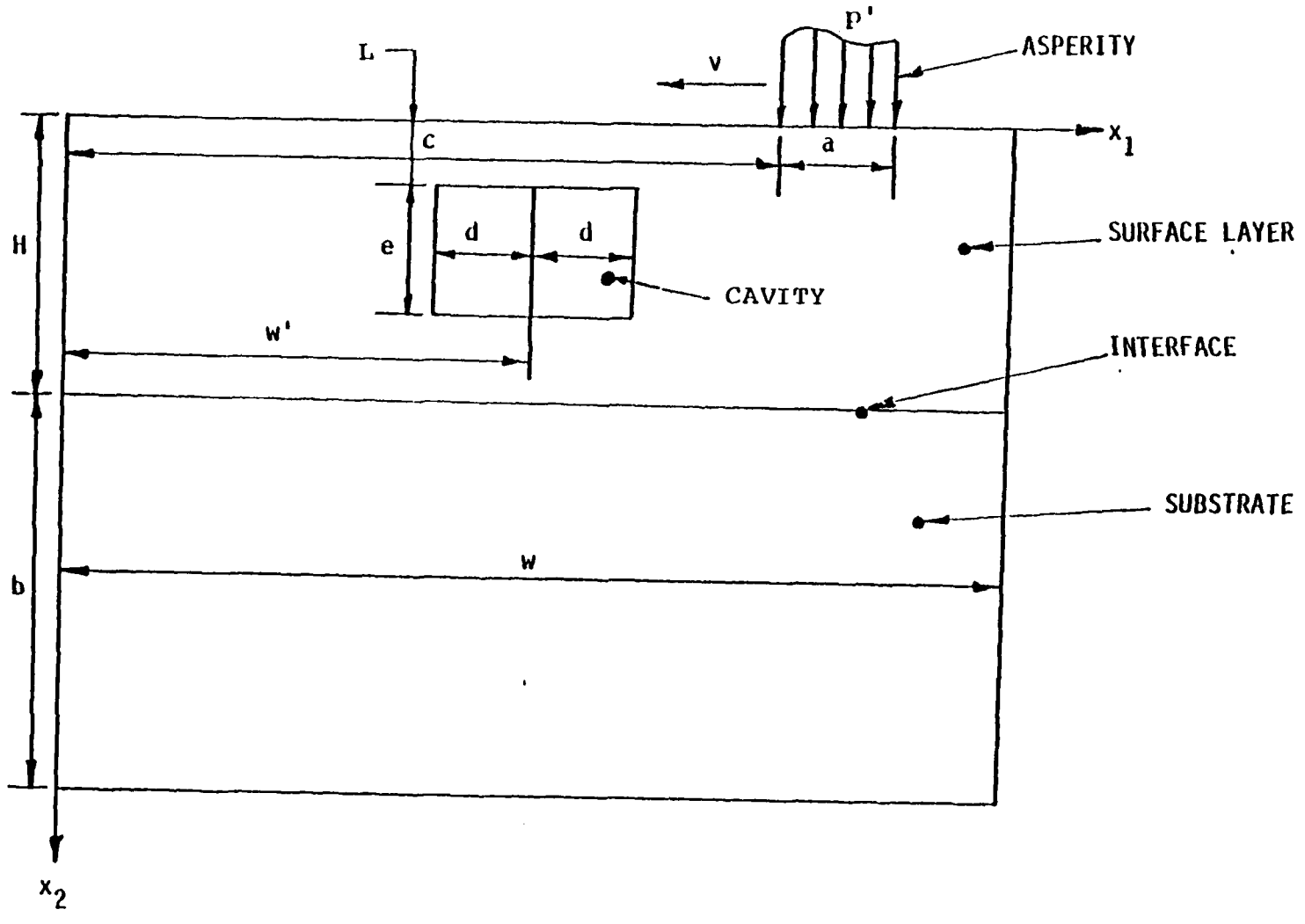

Figure 2. Numerical model.

$$\phi^{(2)}(i,j,n) = \alpha^2 r_1[\phi^{(2)}(i-1,j,n-1) + \phi^{(2)}(i+1,j,n-1)] +$$

$$+ [1 - 2\alpha^2(r_1+r_2)]\phi^{(2)}(i,j,n-1) +$$

$$+ \alpha^2 r_2[\phi^{(2)}(i,j-1,n-1) + \phi^{(2)}(i,j+1,n-1)], \qquad (11)$$

where $r_1 = \Delta\tau/(R_1 \cdot \Delta\xi^2)$, $r_2 = \Delta\tau/(R_1 \cdot \Delta\eta^2)$, $\alpha^2 = \kappa_2/\kappa_1$, and (i,j,n) denotes the two spatial indices and the time step respectively. The stability criteria for the explicit scheme can be shown to be

$$1 - 2(r_1+r_2) \geq 0, \qquad (12)$$

$$1 - 2\alpha^2(r_1+r_2) \geq 0. \qquad (13)$$

If α^2 is less than 1, Equation (12) is the stability criterion, otherwise Equation (13) is the stability criterion for the explicit scheme.

Based on the previous works [1,2,3,6,10], we know that the high temperature and the high thermal stresses occur in the region near the asperity. Therefore, in that region one must use very fine mesh to obtain good results. But for those locations far away from the asperity, one can use coarse mesh in order to save computing time. This non-uniform mesh can be taken care of by applying the general coordinates transformation [13] (Fig. 3). The derivatives of a function $f(\bar{\xi},\bar{\eta})$ in the transformed plane $(\bar{\xi},\bar{\eta})$ are:

$$f_\xi = (\eta_{\bar{\eta}}\, f_{\bar{\xi}} - \eta_{\bar{\xi}}\, f_{\bar{\eta}})/J \ , \qquad (14)$$

$$f_\eta = (\xi_{\bar{\xi}}\, f_{\bar{\eta}} - \xi_{\bar{\eta}}\, f_{\bar{\xi}})/J \ , \qquad (15)$$

$$f_{\xi\xi} = (\eta_{\bar{\eta}}^2\, f_{\bar{\xi}\bar{\xi}} - 2\eta_{\bar{\xi}}\, \eta_{\bar{\eta}}\, f_{\bar{\xi}\bar{\eta}} + \eta_{\bar{\xi}}^2\, f_{\bar{\eta}\bar{\eta}})/J^2$$

$$+ [(\eta_{\bar{\eta}}^2\, \eta_{\bar{\xi}\bar{\xi}} - 2\eta_{\bar{\xi}}\, \eta_{\bar{\eta}}\, \eta_{\bar{\xi}\bar{\eta}} + \eta_{\bar{\xi}}^2\, \eta_{\bar{\eta}\bar{\eta}})(\xi_{\bar{\eta}}\, f_{\bar{\xi}} - \xi_{\bar{\xi}}\, f_{\bar{\eta}})$$

$$+ (\eta_{\bar{\eta}}^2\, \xi_{\bar{\xi}\bar{\xi}} - 2\eta_{\bar{\xi}}\, \eta_{\bar{\eta}}\, \xi_{\bar{\xi}\bar{\eta}} + \eta_{\bar{\xi}}^2\, \xi_{\bar{\eta}\bar{\eta}})(\eta_{\bar{\xi}}\, f_{\bar{\eta}} - \eta_{\bar{\eta}}\, f_{\bar{\xi}})]/J^3, \qquad (16)$$

GENERAL COORDINATES TRANSFORMATION

$(\xi, \eta) \rightarrow (\bar{\xi}, \bar{\eta})$

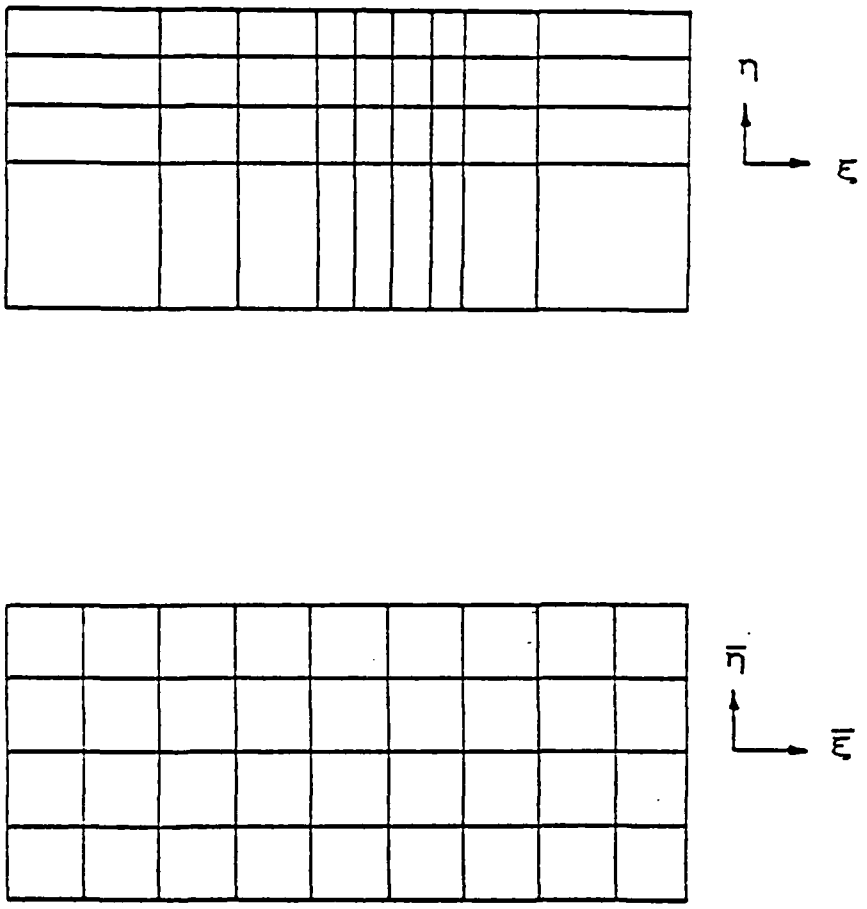

Figure 3. General coordinates transformation.

$$f_{\eta\eta} = (\xi_{\eta}^{-2} f_{\bar{\xi}\bar{\xi}} - 2\xi_{\bar{\xi}} \xi_{\eta} f_{\bar{\xi}\eta} + \xi_{\bar{\xi}}^{2} f_{\eta\eta})/J^2$$
$$+ [(\xi_{\eta}^{-2} \eta_{\bar{\xi}\bar{\xi}} - 2\xi_{\bar{\xi}} \xi_{\eta} \eta_{\bar{\xi}\eta} + \xi_{\bar{\xi}}^{2} \eta_{\eta\eta}) (\xi_{\eta} f_{\bar{\xi}} - \xi_{\bar{\xi}} f_{\eta})$$
$$+ (\xi_{\eta}^{-2} \xi_{\bar{\xi}\bar{\xi}} - 2\xi_{\bar{\xi}} \xi_{\eta} \xi_{\bar{\xi}\eta} + \xi_{\bar{\xi}}^{2} \xi_{\eta\eta}) (\eta_{\bar{\xi}} f_{\eta} - \eta_{\eta} f_{\bar{\xi}})]/J^3, \quad (17)$$

where $J = \xi_{\bar{\xi}} \eta_{\eta} - \xi_{\eta} \eta_{\bar{\xi}}$ is the Jacobian of the transformation, the subscripts $(\xi,\eta,\bar{\xi},\bar{\eta})$ denotes partial derivatives in those coordinates respectively.

The heat conduction Equations (1,2) in the transformed plane can be written as

$$(A_1 \phi_{\xi\xi}^{(i)} - 2A_2 \phi_{\xi\eta}^{(i)} + A_3 \phi_{\eta\eta}^{(i)} + A_4 \phi_{\eta}^{(i)} + A_5 \phi_{\xi}^{(i)})/J^2 = R_i \phi^{(i)} ,$$
$$i = 1,2 \quad (18)$$

where

$$A_1 = \xi_{\eta}^{-2} + \eta_{\eta}^{-2} , \quad (19)$$

$$A_2 = \xi_{\bar{\xi}} \xi_{\eta} + \eta_{\bar{\xi}} \eta_{\eta} , \quad (20)$$

$$A_3 = \xi_{\bar{\xi}}^{2} + \eta_{\eta}^{-2} , \quad (21)$$

$$A_4 = (\eta_{\bar{\xi}} A_6 - \xi_{\bar{\xi}} A_7)/J , \quad (22)$$

$$A_5 = (\xi_{\eta} A_7 - \eta_{\eta} A_6)/J , \quad (23)$$

$$A_6 = A_1 \xi_{\bar{\xi}\bar{\xi}} - 2A_2 \xi_{\bar{\xi}\eta} + A_3 \xi_{\eta\eta} , \quad (24)$$

$$A_7 = A_1 \eta_{\bar{\xi}\bar{\xi}} - 2A_2 \eta_{\bar{\xi}\eta} + A_3 \eta_{\eta\eta} . \quad (25)$$

At the outer boundaries of the rectangular region (excluding the surface), $\phi = 0$ is the nominal value. The remaining conditions, on the surface, the cavity boundaries and at the interface, shall be incorporated with an energy balance scheme [14].

2.3 Energy Balance

The cavity boundaries, the moving asperity and the interface of the medium are taken care of with the use of the energy balance method.

(i) Energy balance at the interface (see Fig. 4).

For the material 1 (surface layer), the heat fluxes toward the point P at the interface from material points M, R and S in the surface layer are

$$Q_{M\to P} = k_1(\Delta y/2)\,\frac{T(i-1,j) - T(i,j)}{\Delta x}\,, \tag{26}$$

$$Q_{R\to P} = k_1(\Delta y/2)\,\frac{T(i+1,j) - T(i,j)}{\Delta x}\,, \tag{27}$$

$$Q_{S\to P} = k_1(\Delta x)\,\frac{T(i,j-1) - T(i,j)}{} \tag{28}$$

For the material 2 (substrate), the heat fluxes toward the interface point P from material points M, R and N in the substrate region are

$$Q_{M\to P} = k_2(\Delta y/2)\,\frac{T(i-1,j) - T(i,j)}{\Delta x}\,, \tag{29}$$

$$Q_{R\to P} = k_2(\Delta y/2)\,\frac{T(i+1,j) - T(i,j)}{\Delta x}\,, \tag{30}$$

$$Q_{N\to P} = k_2(\Delta x)\,\frac{T(i,j+1) - T(i,j)}{\Delta y}\,, \tag{31}$$

where Q is the heat flux, indexed by the flow direction.

The total heat flux goes in the interface point P(i,j) is

$$Q_{sum} = (k_1+k_2)\,(\Delta y/2)\left[\frac{T(i-1,j) - T(i,j)}{\Delta x} + \frac{T(i+1,j) - T(i,j)}{\Delta x}\right] + \\ + k_1\,(\Delta x)\,\frac{T(i,j-1) - T(i,j)}{\Delta y} + k_2\,(\Delta x)\,\frac{T(i,j+1) - T(i,j)}{\Delta y}\,. \tag{32}$$

The rate of change of internal energy $\dot{U}$ in the time interval Δt and in the neighborhood of P(i,j) is

$$\dot{U} = \dot{U}_1 + \dot{U}_2 = \\ = [\rho_1 c_1(0.5\,\Delta x\cdot\Delta y) + \rho_2 c_2(0.5\,\Delta x\cdot\Delta y)]\,\frac{T(i,j,n) - T(i,j,n-1)}{\Delta t}\,. \tag{33}$$

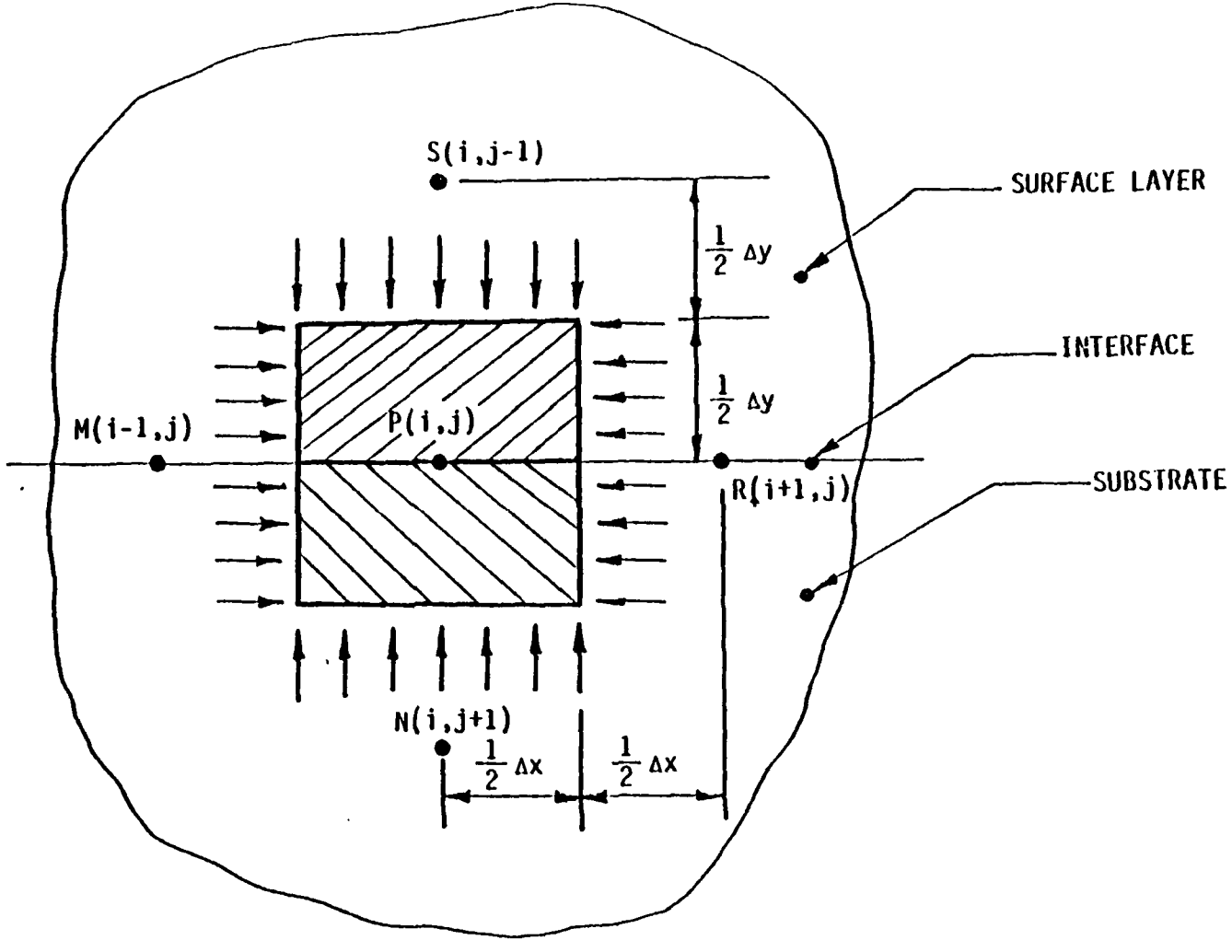

Figure 4. Energy balance at the interface.

For conservation of energy, $\dot{U} = Q_{sum}$, one obtains the equation for the continuity condition at the interface point P(i,j) at the time step n is

$$T(i,j,n) = \left[1 - \frac{2(k_1+k_2)}{(\rho_1 c_1+\rho_2 c_2)} \cdot \frac{\Delta t}{\Delta x^2} - \frac{2(k_1+k_2)}{(\rho_1 c_1+\rho_2 c_2)} \cdot \frac{\Delta t}{\Delta y^2}\right] T(i,j,n-1) +$$

$$+ \frac{(k_1+k_2)}{(\rho_1 c_1+\rho_2 c_2)} \cdot \frac{\Delta t}{\Delta x^2} [T(i-1,j,n-1) + T(i+1,j,n-1)] +$$

$$+ \frac{2k_1}{(\rho_1 c_1+\rho_2 c_2)} \cdot \frac{\Delta t}{\Delta y^2} T(i,j-1,n-1) +$$

$$+ \frac{2k_2}{(\rho_1 c_1+\rho_2 c_2)} \cdot \frac{\Delta t}{\Delta y^2} T(i,j+1,n-1) . \qquad (34)$$

Equation (34) in dimensionless form is

$$\phi(i,j,n) = \left[1 - \frac{2(1+\beta)}{(1+\beta/\alpha^2)} r_1 - \frac{2(1+\beta)}{(1+\beta/\alpha^2)} r_2\right] \phi(i,j,n-1)$$

$$+ \frac{(1+\beta)}{(1+\beta/\alpha^2)} r_1 [\phi(i-1,j,n-1) + \phi(i+1,j,n-1)]$$

$$+ \frac{2}{(1+\beta/\alpha^2)} r_2 \phi(i,j-1,n-1) + \frac{2\beta}{(1+\beta/\alpha^2)} r_2 \phi(i,j+1,n-1) , \qquad (35)$$

where $\beta = k_2/k_1$.

(ii) Energy balance on the cavity boundaries (Fig. 5). The heat fluxes toward the boundary point P(i,j) from the material points M, S and N are

$$Q_{M\to P} = k(\Delta y) \frac{T(i-1,j) - T(i,j)}{\Delta x} , \qquad (36)$$

$$Q_{S\to P} = k(\Delta x/2) \frac{T(i,j-1) - T(i,j)}{\Delta y} , \qquad (37)$$

$$Q_{N\to P} = k(\Delta x/2) \frac{T(i,j+1) - T(i,j)}{\Delta y} . \qquad (38)$$

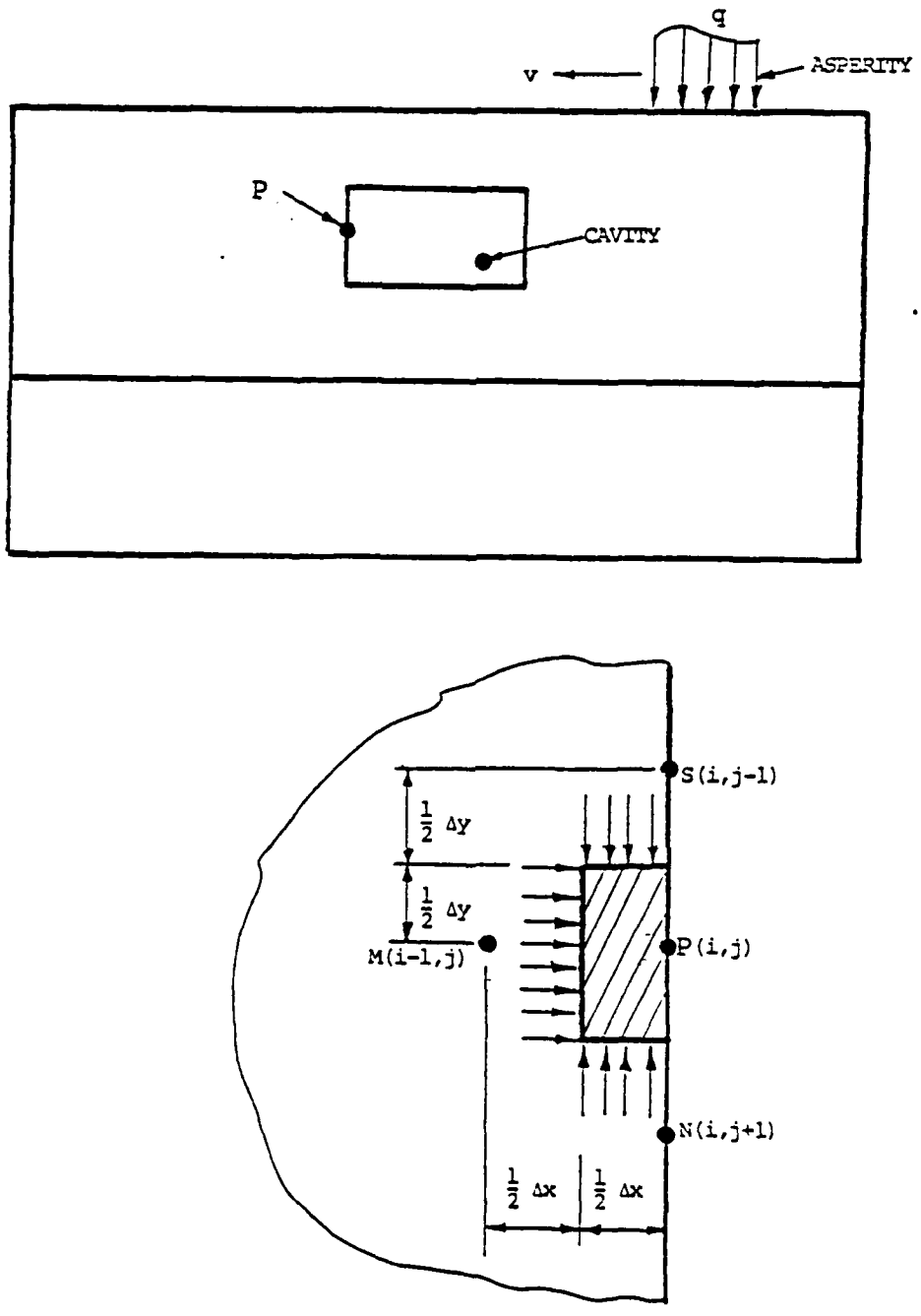

Figure 5. Energy balance on the cavity boundaries.

The total heat input at P(i,j) is then:

$$Q_{sum} = Q_{M\to P} + Q_{S\to P} + Q_{N\to P} = k(\Delta y)\ \frac{T(i-1,j) - T(i,j)}{\Delta x} + \tag{39}$$
$$+ k(\Delta x/2)\ \frac{T(i,j+1) - T(i,j)}{\Delta y} + k(\Delta x/2)\ \frac{T(i,j+1) - T(i,j)}{\Delta y} .$$

The rate of internal energy increase in the neighborhood of P(i,j) is

$$\dot{U} = \rho c\ (0.5\ \Delta x\ \Delta y)\ \frac{T(i,j,n) - T(i,j,n-1)}{\Delta t} . \tag{40}$$

From conservation of energy, one can obtain the temperature at the boundary point P(i,j) at the time step n:

$$T(i,j,n) = T(i,j,n-1) + \frac{2k\Delta t}{\rho c}\ \left[\frac{T(i-1,j,n-1) - T(i,j,n-1)}{\Delta x^2} + \right.$$
$$\left. + 0.5\ \frac{T(i,j-1,n-1) - 2T(i,j,n-1) + T(i,j+1,n-1)}{\Delta y^2}\right] . \tag{41}$$

Equation (41) in dimensionless form is

$$\theta(i,j,n) = \theta(i,j,n-1) + 2r_1[\theta(i-1,j,n-1) - \theta(i,j,n-1)] +$$
$$+ r_2[\theta(i,j-1,n-1) - 2\theta(i,j,n-1) + \theta(i,j+1,n-1)] . \tag{42}$$

Similarly, other points on the cavity boundaries can be obtained.

(iii) Energy balance at the corner of the cavity.

The points at the four corners of the cavity are singularities because at each of those four points there are two boundary conditions, $\partial_1 T = \partial_2 T = 0$, with only one unknown T. However by applying an energy balance scheme, one can resolve such problems at the corner (see Fig. 6). The heat fluxes toward the corner point P(i,j) are:

$$Q_{M\to P} = k(\Delta y)\ \frac{T(i-1,j) - T(i,j)}{\Delta x} , \tag{43}$$

$$Q_{N\to P} = k(\Delta x/2)\ \frac{T(i,j+1) - T(i,j)}{\Delta y} , \tag{44}$$

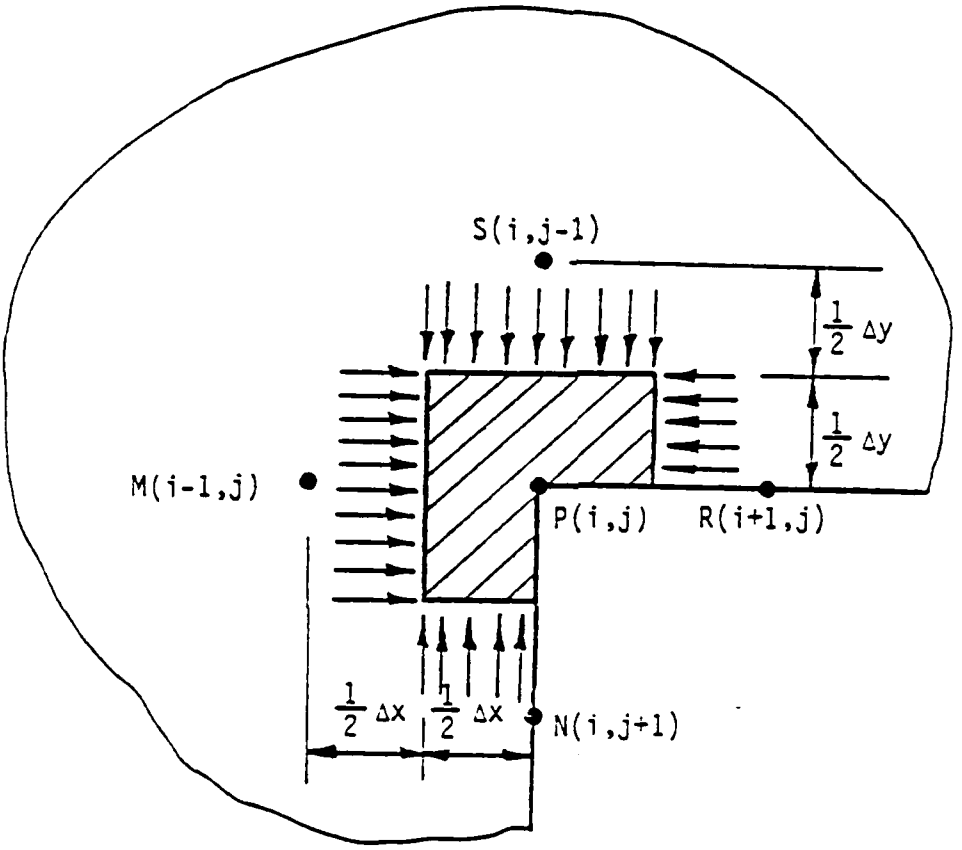

Figure 6. Energy balance on the corner point of the cavity.

$$Q_{R\to P} = k(\Delta y/2)\ \frac{T(i+1,j) - T(i,j)}{\Delta x}\ , \tag{45}$$

$$Q_{S\to P} = k(\Delta x)\ \frac{T(i,j-1) - T(i,j)}{\Delta y}\ . \tag{46}$$

The total heat input at P(i,j) is therefore

$$Q_{sum} = k(\Delta y)\ \frac{T(i-1,j) - T(i,j)}{\Delta x} + k(\Delta x/2)\ \frac{T(i,j+1) - T(i,j)}{\Delta y} + \\ + k(\Delta y/2)\ \frac{T(i+1,j) - T(i,j)}{\Delta x} + k(\Delta x)\ \frac{T(i,j-1) - T(i,j)}{\Delta y}\ . \tag{47}$$

The rate of increase in internal energy is

$$\dot{U} = \rho c(0.5\ \Delta x\ \Delta y + 0.25\ \Delta x\ \Delta y)\ \frac{T(i,j,n) - T(i,j,n-1)}{\Delta t}\ . \tag{48}$$

From conservation of energy, the equation for boundary conditions at the corner point P(i,j) is therefore

$$T(i,j,n) = T(i,j,n-1) + (4/3)\ (k/\rho c)\ (\Delta t/\Delta x^2)\ [T(i-1,n-1) - \\ - (3/2)\ T(i,j,n-1) + (1/2)\ T(i+1,j,n-1)] + \\ + (4/3)\ (k/\rho c)\ (\Delta t/\Delta y^2)\ [T(i,j-1,n-1) - \\ - (3/2)\ T(i,j,n-1) + (1/2)\ T(i,j+1,n-1)]\ . \tag{49}$$

Equation (49) in dimensionless form is

$$\theta(i,j,n) = \theta(i,j,n-1) + (4/3)r_1[\theta(i-1,j,n-1) - 1.5\ \theta(i,j,n-1) + \\ + 0.5\ \theta(i+1,j,n-1)] + (4/3)r_2[\theta(i,j-1,n-1) - \\ - 1.5\ \theta(i,j,n-1) + 0.5\ \theta(i,j+1,n-1)]\ . \tag{50}$$

Similarly, the boundary conditions at the other corner points of the cavity are obtained.

(iv) Energy balance on the surface boundary (under the moving asperity at the time step n).

For the explicit scheme, the time step is limited by the stability criterion. As a result, the moving asperity at some time may not be right above the grid points. To alleviate this situation, one can also use the energy balance method to describe the boundary condition (see Fig. 7). The heat fluxes toward P from material points M, N and R are

$$Q_{M\to P} = k(\Delta y/2)\ \frac{T(i-1,1) - T(i,1)}{\Delta x}\ , \tag{51}$$

$$Q_{N\to P} = k(\Delta x)\ \frac{T(i,2) - T(i,1)}{\Delta y}\ , \tag{52}$$

$$Q_{R\to P} = k(\Delta y/2)\ \frac{T(i+1,1) - T(i,1)}{\Delta x}\ . \tag{53}$$

The exterior heat flux in the neighborhood surface of the boundary point P(i,j), which is under the asperity at the time n, is

$$Q_{ext\to P} = q(0.5\ \Delta x + h)/\text{unit thickness}$$

where h is less than $\Delta x/2$. The formulation thus takes care of all cases when the asperity end points do not fall on a material grid point on the boundary. The total heat input at P is therefore

$$Q_{sum} = k\left[(\Delta y/2)\ \frac{T(i-1,1) - T(i,1)}{\Delta x} + (\Delta x)\ \frac{T(i,2) - T(i,1)}{\Delta y} + \right.$$

$$\left. + (\Delta y/2)\ \frac{T(i+1,1) - T(i,1)}{\Delta x}\right] + q(0.5\ \Delta x + h)\ . \tag{55}$$

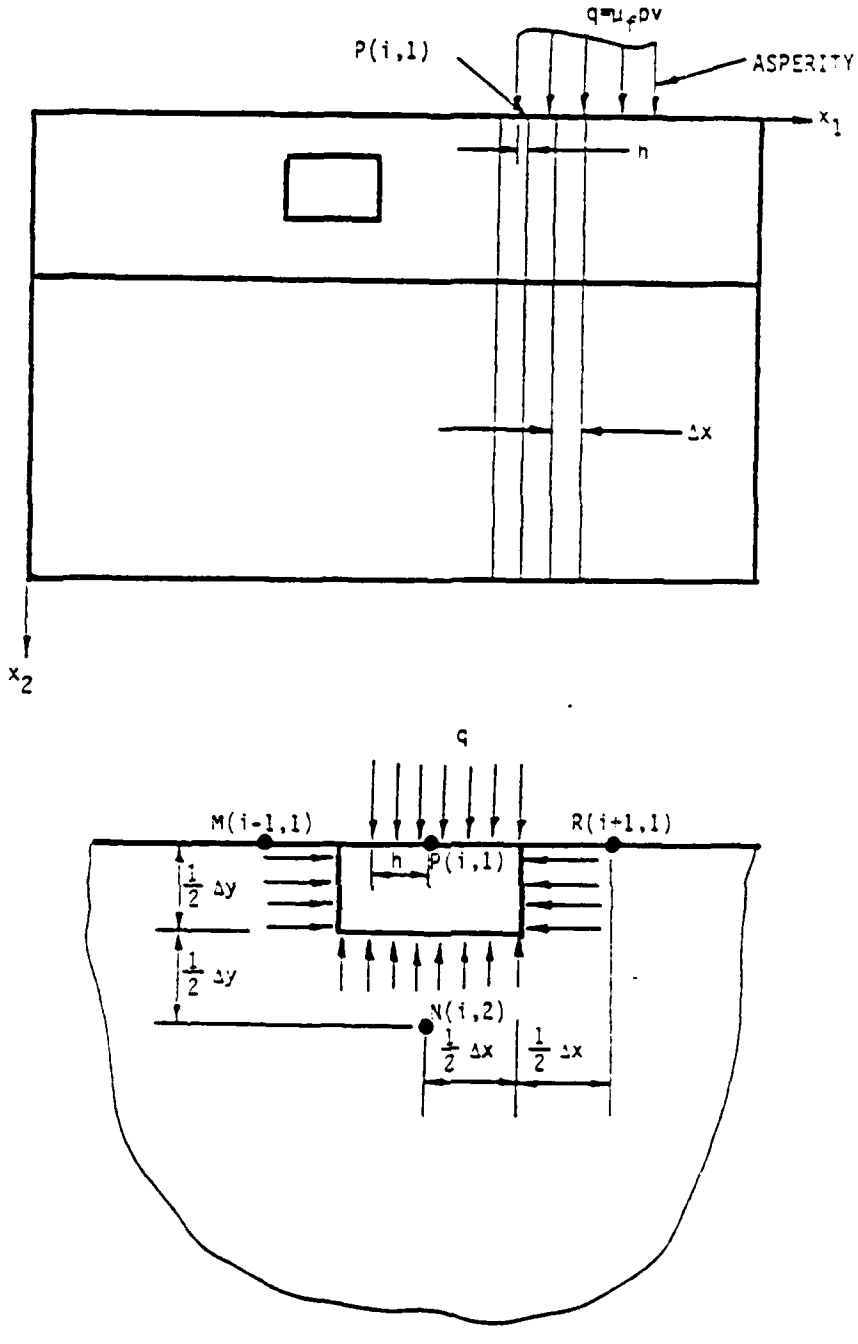

Figure 7. Engergy balance on the surface.

The rate of increase of the internal energy in the neighborhood of P(i,j) is

$$\dot{U} = \rho c\,(0.5\,\Delta x\,\Delta y)\,\frac{T(i,j,n) - T(i,j,n-1)}{\Delta t}\,. \qquad (56)$$

The condition on the surface boundary with the use of the conservation of energy becomes

$$T(i,1,n) = T(i,1,n-1) + (k/\rho c)\,(\Delta t/\Delta x^2)\,[T(i-1,1,n-1) - 2T(i,1,n-1) + T(i+1,1,n-1)] + (2k/\rho c)\,(\Delta t/\Delta y^2)\,[T(i,2,n-1) - T(i,1,n-1)] + \frac{2q(0.5\,\Delta x + h)\Delta t}{\rho c\,\Delta x\,\Delta y}\,. \qquad (57)$$

Equation (57) in dimensionless form is

$$\phi(i,1,n) = \phi(i,1,n-1) + r_1[\phi(i-1,1,n-1) - 2\phi(i,1,n-1) + \phi(i+1,1,n-1)] + 2r_2[\phi(i,2,n-1) - \phi(i,1,n-1)] + (1+h')\,\frac{\Delta\tau}{R\Delta\eta}\,, \qquad (58)$$

where $h' = h/(\Delta x/2)$.

Equations (10,11,35,42,50,58) constitute the general formulation of the problem with a complete set of difference equations for the solutions of the discrete temperature field $\{\phi(i,j,n)\}$ at some specific time.

CHAPTER III

NUMERICAL RESULTS

Numerical results are obtained by using the non-uniform rectangular mesh corresponding to different cases of material properties and geometry. For the surface layer of Silicon Carbide, $k_1 = 1.047$ J/cm.°C.s, $\kappa_1 = 0.49$ cm^2/s, and $c_1 = 712$ J/kg.°C. For the substrate of Aluminum, $k_2 = 2.02$ J/cm.°C.s, $\kappa_2 = 0.961$ cm^2/s, and $c_2 = 917$ J/kg.°C. The other numerical parameters on the asperity and the cavity are: $v = 15$ ms^{-1}, $w = 4a$, $H = 1.2a$, $E = 1.9a$, $d = 0.3a$, $e = 0.5a$, $a = 1$mm, the smallest $\Delta\xi$ and $\Delta\eta$ are 0.02 and 0.01 respectively, and $\Delta\tau = 0.01$. At the limiting case of no cavity, the maximum dimensionless temperature at surface of the coated media was found to be 0.124 by using the transform method [1]. The result at the same point by the current finite difference formulation is 0.123. The error is less than 1%. The numerical scheme is therefore confirmed by the benchmark problem.

The solutions for a single material with and without a cavity would then be compared with two limiting cases. For the first case, the cavity is located entirely in the surface layer, Figure 8a. In the second case, the top edge of the cavity is at the layer/substrate interface, Figure 8b. The solutions for the single material without and with a cavity are designated as the third and the fourth cases respectively, included for the purpose of comparison. In Case 1, three different values of the ligament thickness: 0.04 (Case 1A), 0.06 (Case 1B) and 0.1 (Case 1E), are used to illustrate the effect of the ligament volume. The temperature fields at two depths, for all three Cases 1A, 1B and 1E are shown in Figure 9. In the figure, the

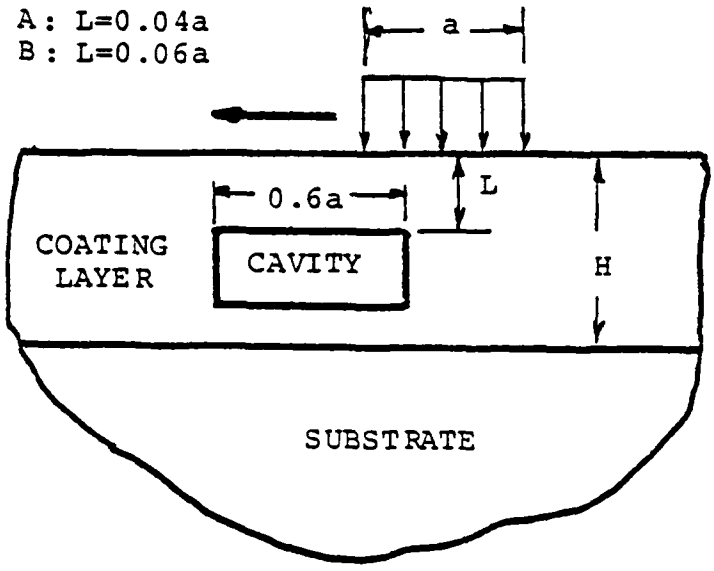

CASE 1
(a)

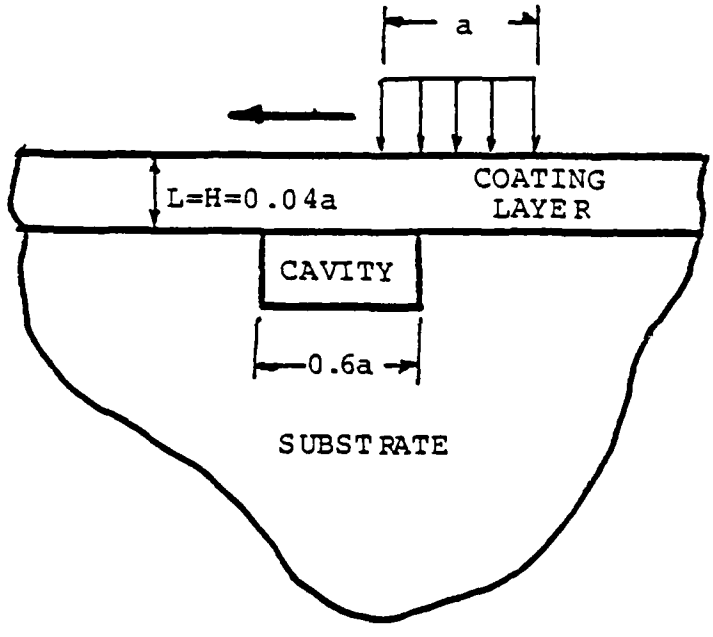

CASE 2
(b)

Figure 8. Numerical examples with different cavity positions.

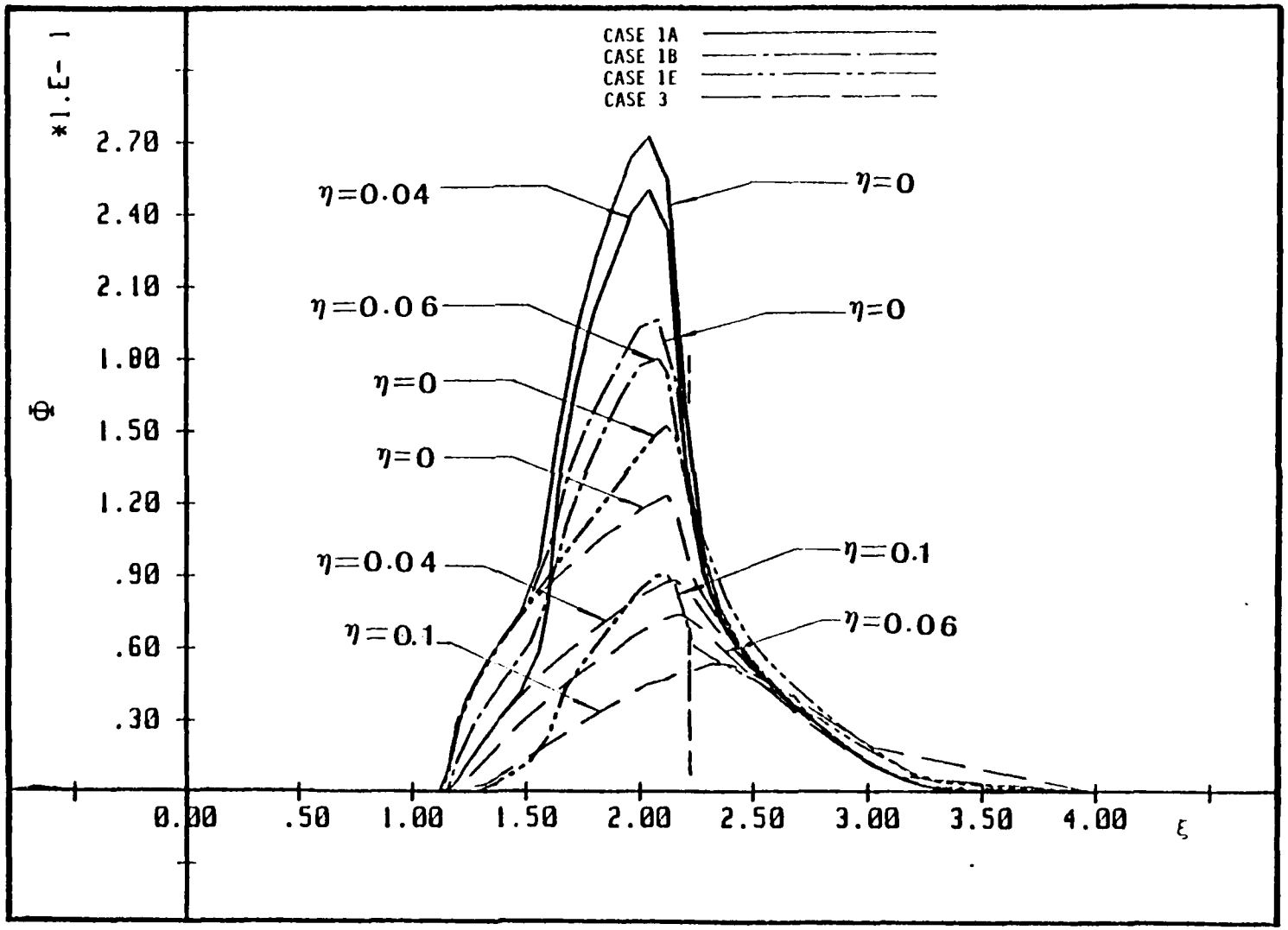

Figure 9. Dimensionless temperature field. Case 1A - coated material with a cavity, cavity is located in the surface layer, L=0.04a. Case 1B - coated material with a cavity, cavity is located in the surface layer, L=0.06a. Case 1E - coated material with a cavity, cavity is located in the surface layer, L=0.1a. Case 3 - single material without cavity.

cavity width is from $\xi = 1.6$ to 2.2. The asperity position, at the dimensionless time $\tau = 1.04$, representing the worst case, is from $\xi = 1.2$ to 2.2. The relative positions of the asperity and the cavity is shown in Figure 10.

The Case 1A then is compared with Case 2 of the same ligament thickness for which the top edge of the cavity is at the layer/substrate interface. The effect of the relative position of the cavity to the interface is shown in Figure 11. It is noticed that when the top edge of the cavity is at the interface, the temperature field in the region immediately on the trailing edge of the asperity will be affect by the substrate material.

The effect of heat capacity and thermal conductivity of the surface layer for Case 1A is shown in Figure 12. The figure shows the original value as Case 1A. Case 1C represents a reduction of thermal capacity of the surface layer by half. Case 1D shows the result of increase in thermal conductivity of the surface layer by 75%. The thermal conductivity of the surface layer is shown to have little effect on the nondimensional surface temperature. But the real temperature field, $T = q_o a b / k_1$, is lowered with increasing thermal conductivity k_1.

Figures 13 and 14 illustrate the effect of a cavity on the direction of heat flux. The figures show the nondimensional heat flux components in ξ and η directions of single material without cavity (Case 3) and a layered medium with a cavity (Case 1A). From the figures, it is observed that with no cavity the heat flux at $\xi = 2.2$, and $\eta = 0.04$ has a magnitude of 0.7 at an angle of 82° to the wear surface, with cavity, at the same location, the magnitude is increased to 1.5 at an angle 23° to the wear surface. Hence, the existence of the cavity will increase the heat flux tremendously, especially in the ξ direction near the upper trailing corner of the cavity. Figures 13 and 14 demonstrate not only an increase in magnitude of the heat

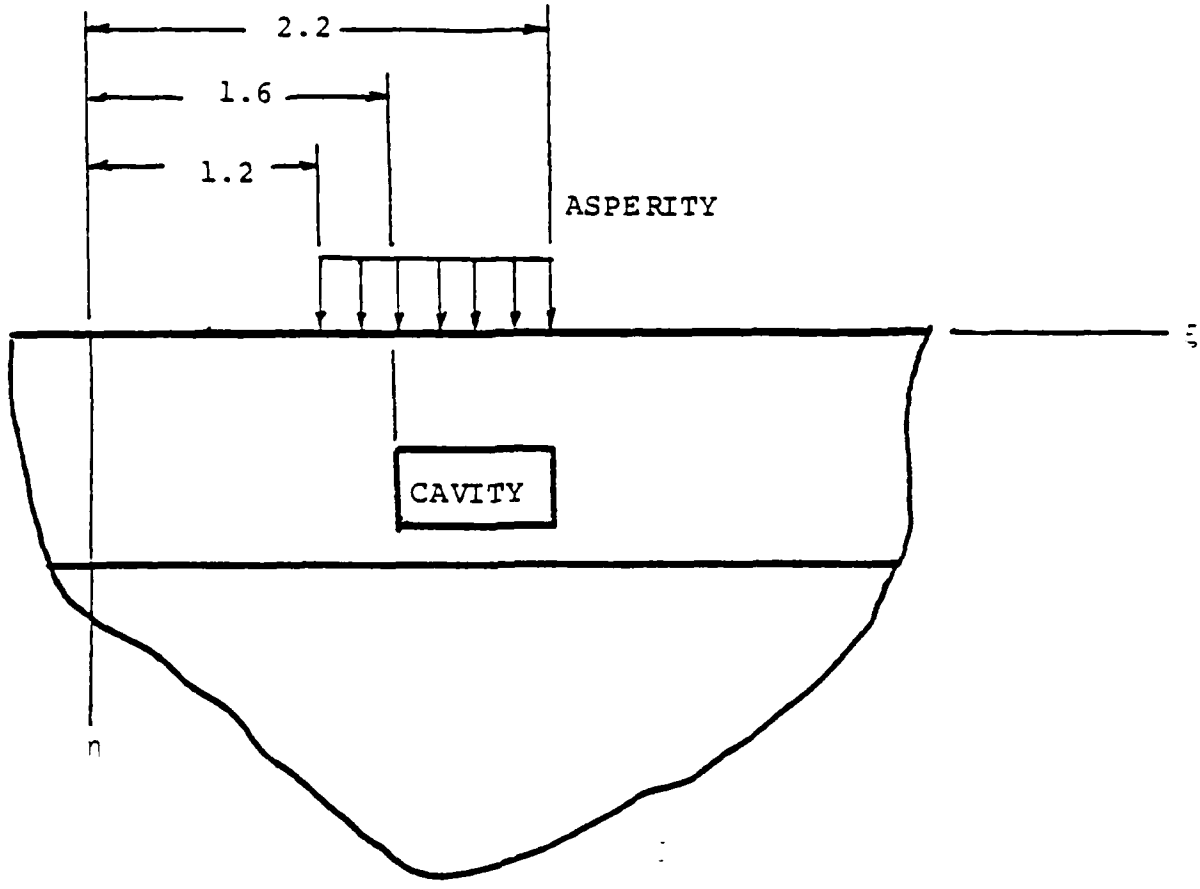

Figure 10. The relative positions of the cavity and the asperity at τ=1.04 the worst case of temperature field.

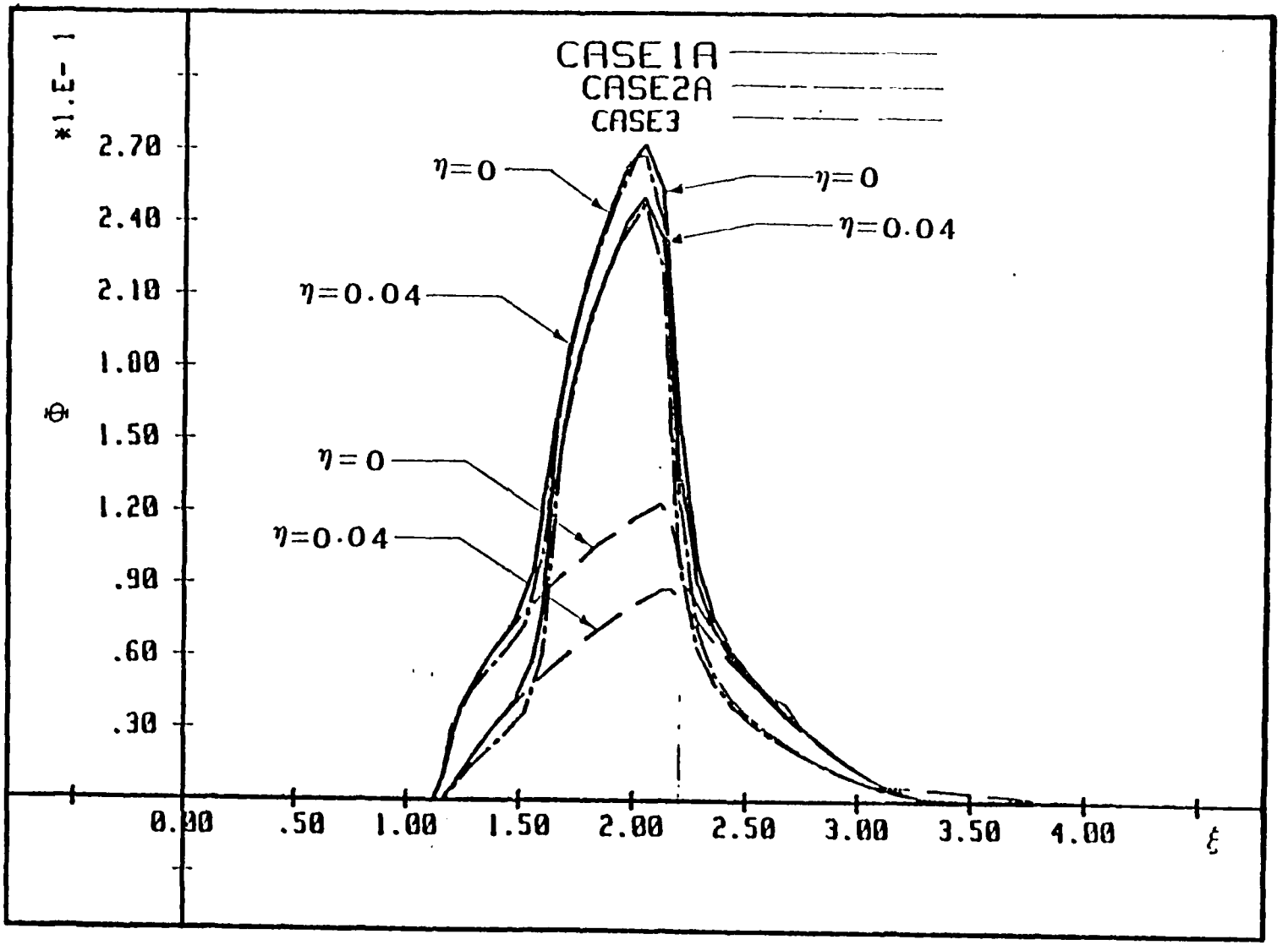

Figure 11. Dimensionless temperature field. Case 2A - coated material with a cavity, the top edge of the cavity is at the interface, L=0.04a.

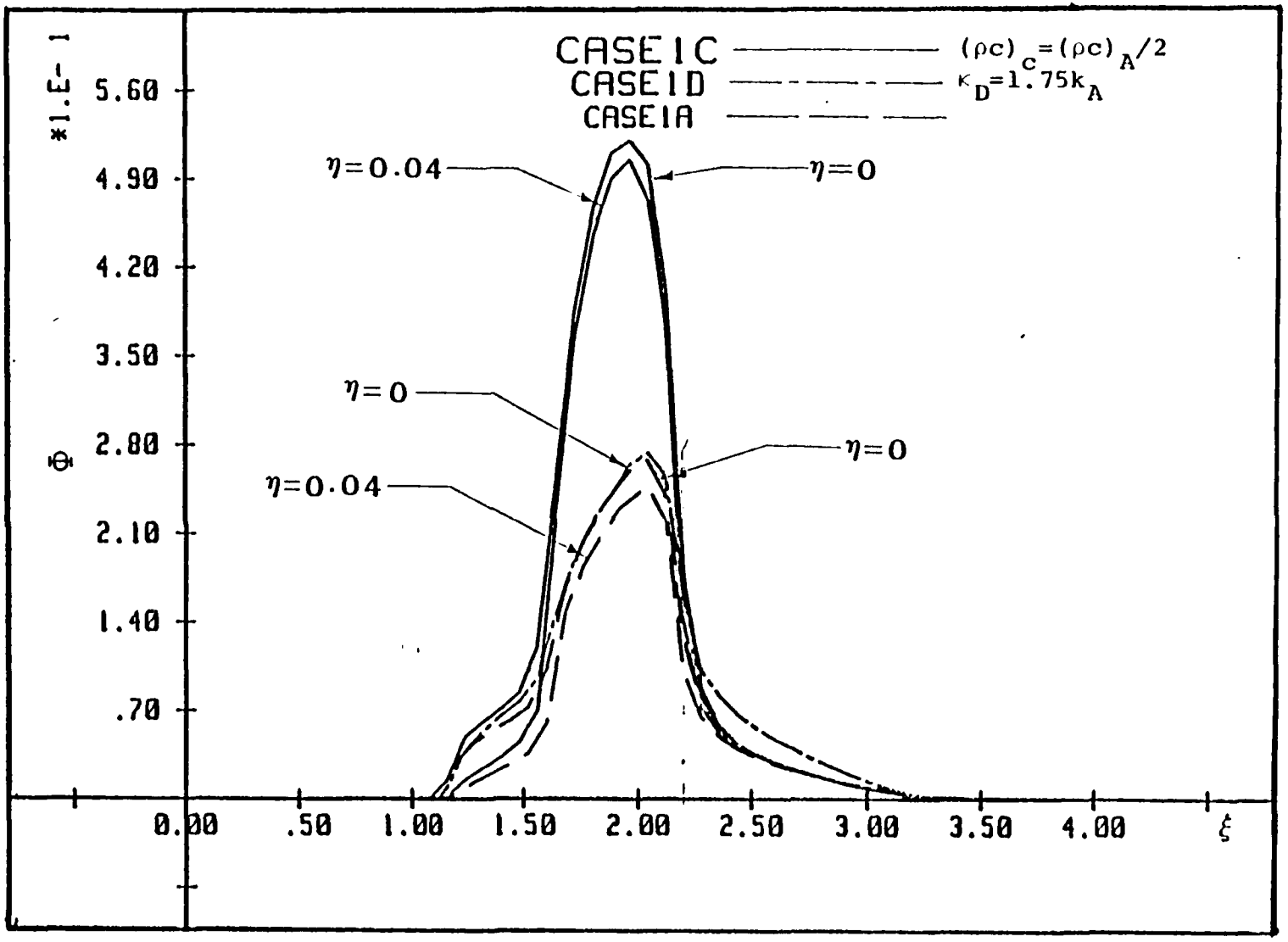

Figure 12. Dimensionless temperature field. Case 1C - the same as Case 1A, except that the thermal capacity of the surface layer is reduced by half. Case 1D - the same as Case 1A, except that the thermal conductivity of the surface layer is increased by 75%.

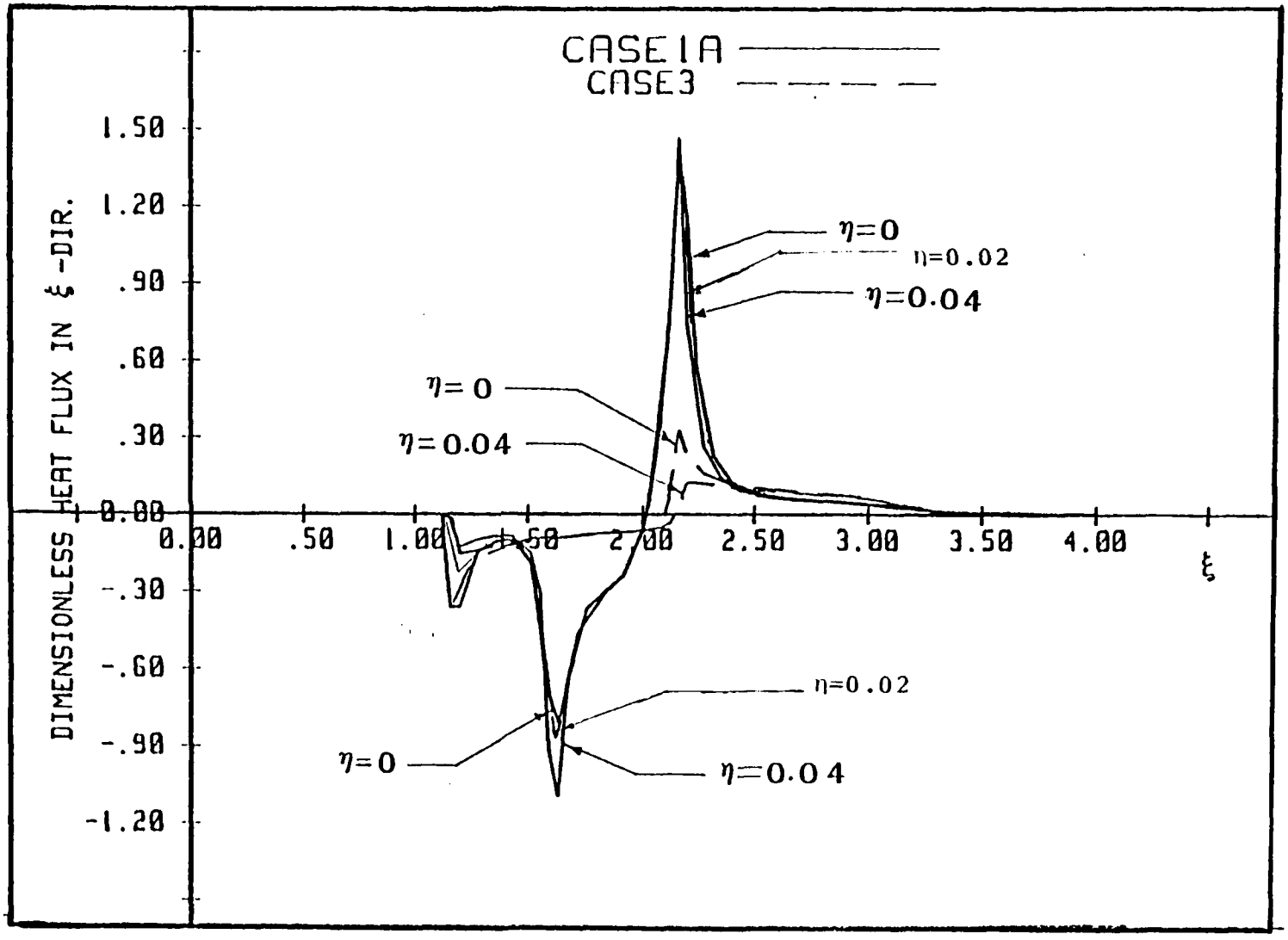

Figure 13. Dimensionless heat flux in ξ-direction.

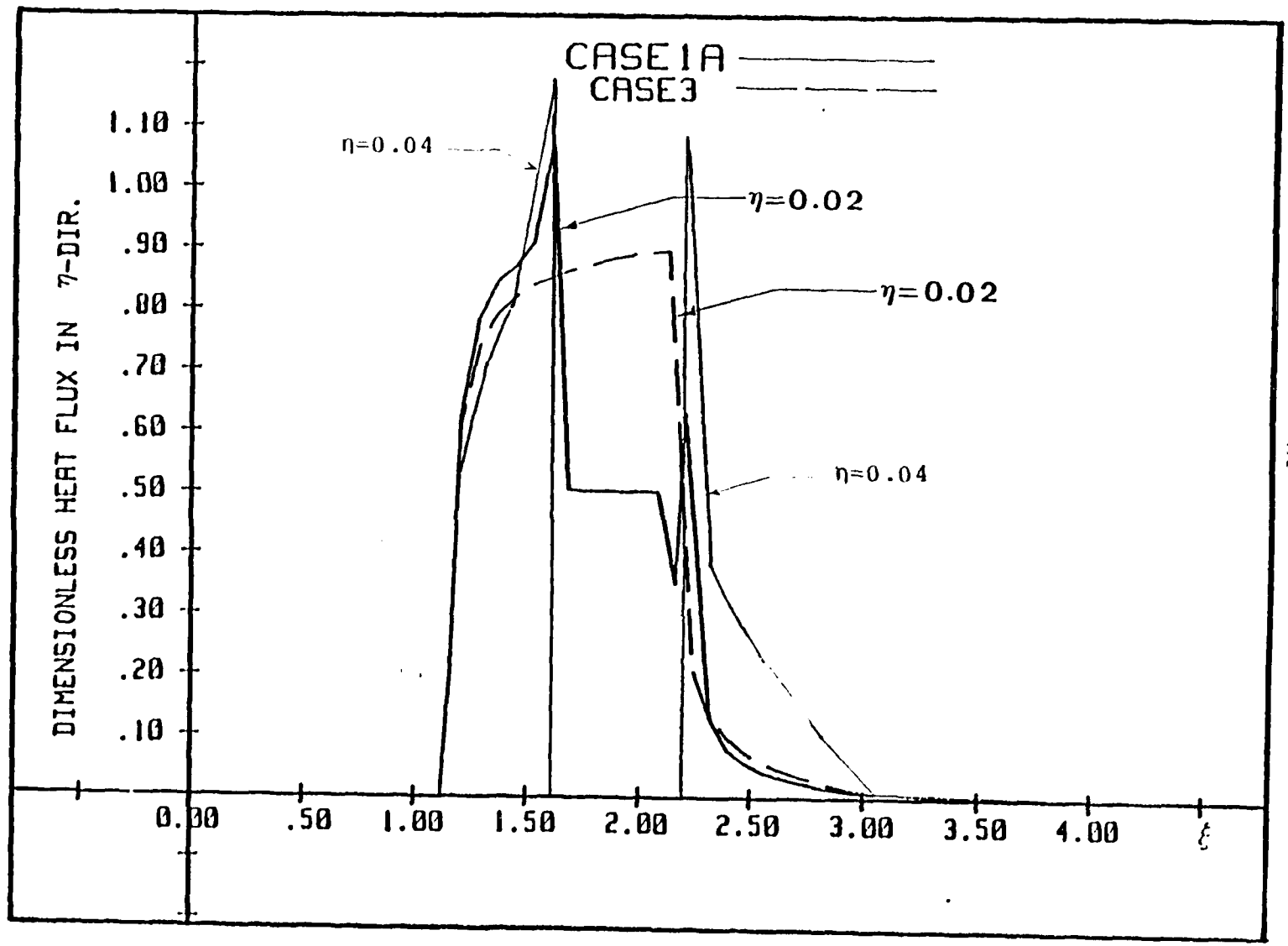

Figure 14. Dimensionless heat flux in η-direction.

flux, hence the temperature gradient, but also the flux at a more oblique angle to the wear surface.

Ju [14] had studied the effect of thermal properties of a single material subjected to the high-speed asperity excitation. It was pointed out that thermal conductivity (k) and thermal capacity (ρc) are the parameters controlling the temperature field. For layered media similar effect was concluded by Ju and Liu [2]. For the case of a layered medium with cavity, the thermal property variation in the coating layer can be accordingly extrapolated. It is the effect of the substrate in the neighborhood of the cavity that would be influential to the temperature field in the critical region. The effect of thermal property variation for the substrate is therefore studied numerically for the Case 2, for which the coating/substrate interface is at the top edge of the cavity. For this case, the thermal properties of the substrate will be immediately influential of the temperature field in the vicinity of the top trailing corner of the cavity. For the purpose demonstration of the individual effect, a benchmark case is chosen for comparison that both the coating and the substrate are of silicon carbide, ($k_1 = k_2 = 1.047$ J/cm.°C.s, $\kappa_1 = \kappa_2 = 0.49$ cm^2/s, $\rho c_1 = \rho c_2 = 2.137$ J/cm^3.C), designated as Case 4. Figure 15 illustrates the temperature field near surface and at the coating/substrate interface for cases with marked changes in thermal properties from those given in Case 4. Case 2B shows no change in the substrate diffusivity, but both the thermal conductivity and the thermal capacity are doubled. The ensuing improved conductivity and capacity in the substrate allow a significant heat flow into the substrate thus a high temperature gradient. The Case 2C, at the same diffusivity but with both the thermal conductivity and the thermal capacity halved, shows a reduced heat flow into the substrate thus a low

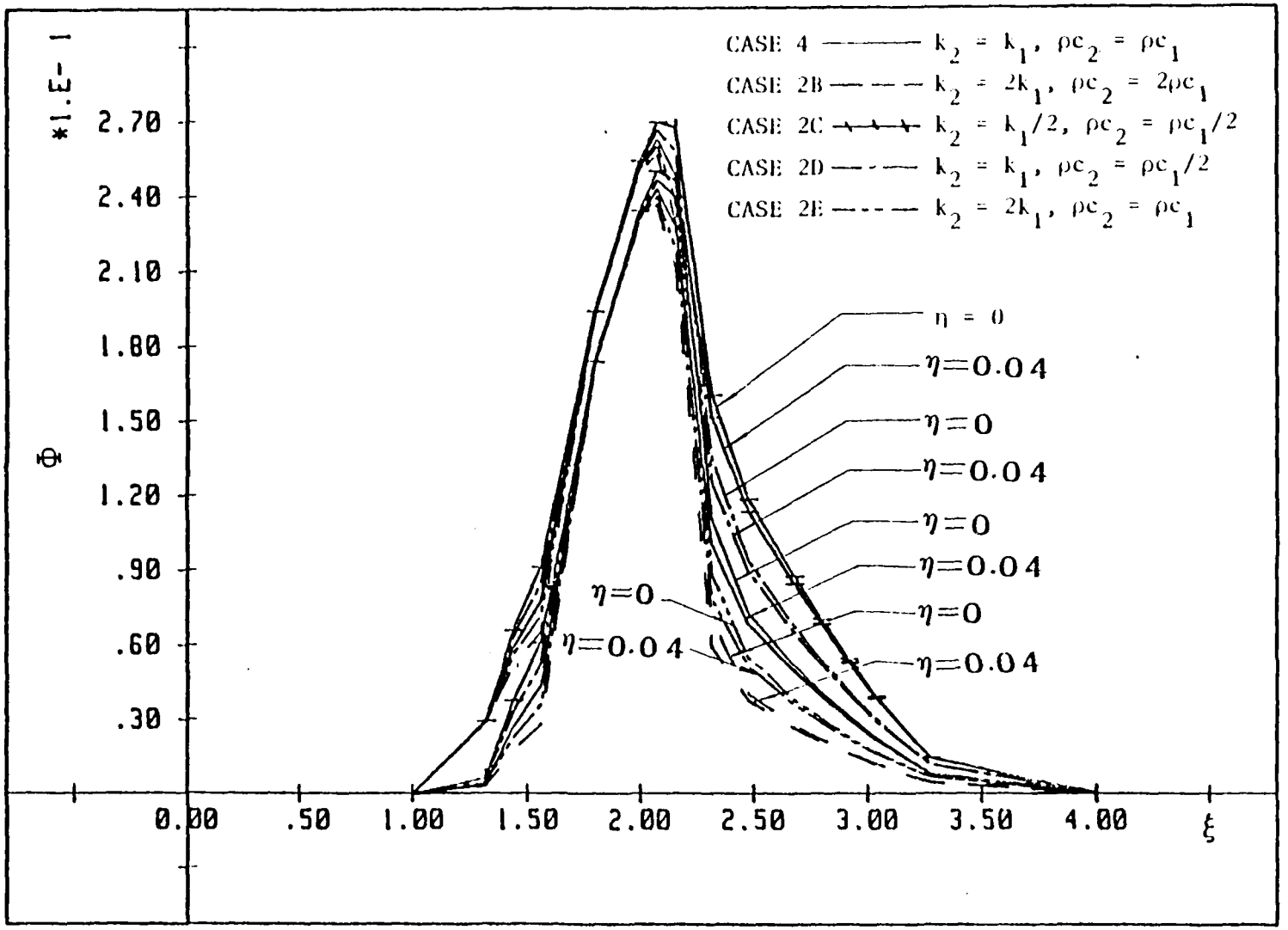

Figure 15. Dimensionless temperature field, showing thermal property effects. Case 2B, 2C, 2D, 2E - coated material with a cavity, the top edge of the cavity is at the interface, showing thermal property changes in comparison to Case 4.

temperature gradient. Cases 2D and 2E, with doubled diffusivity, but from half capacity and double conductivity respectively, showed reduced and increased heat flow into the substrate respectively. The heat flux being proportional to the temperature gradient, is illustrated in Figures 16 and 17 for the surface region and at the interface. It is to be noticed, however, that the temperature gradient and the heat flux are not of identity especially across dissimilar materials. The normal component, to the interface, of the heat flux must be continuous but not the temperature gradient. The tangent component of the temperature gradient must be continuous across the coating/substrate interface. The tangent component of the heat flux, however, is generally not continuous across the interface. In the numerical computation, using the method of energy balance, Equation (32), the x_1-component of heat flux at the coating/substrate interface, Figure 17, is the average of the heat flux components in the coating and the substrate, that is $-0.5(k_1+k_2)\partial T/\partial x_1$.

Figure 18 shows the transient temperature for Case 1A (cavity in the coating and ligament thickness of 0.04) in comparison to the case of a single material without cavity (Case 3). The dimensionless temperatures, $\theta = Tk_1/q_o a$, plotted against the time, $\tau = vt/a$, at surface and at the ligament depth, $\eta = 0.04$, for the position $\xi = 2.2$ where the temperature is maximum in the vicinity of the cavity. It is shown that before the asperity reaches the point, the temperature is low. Then the surface temperature increases and reaches a maximum when the asperity just passes over the trailing edge of the cavity. The temperature at the trailing corner of the cavity lags in time for its peak value.

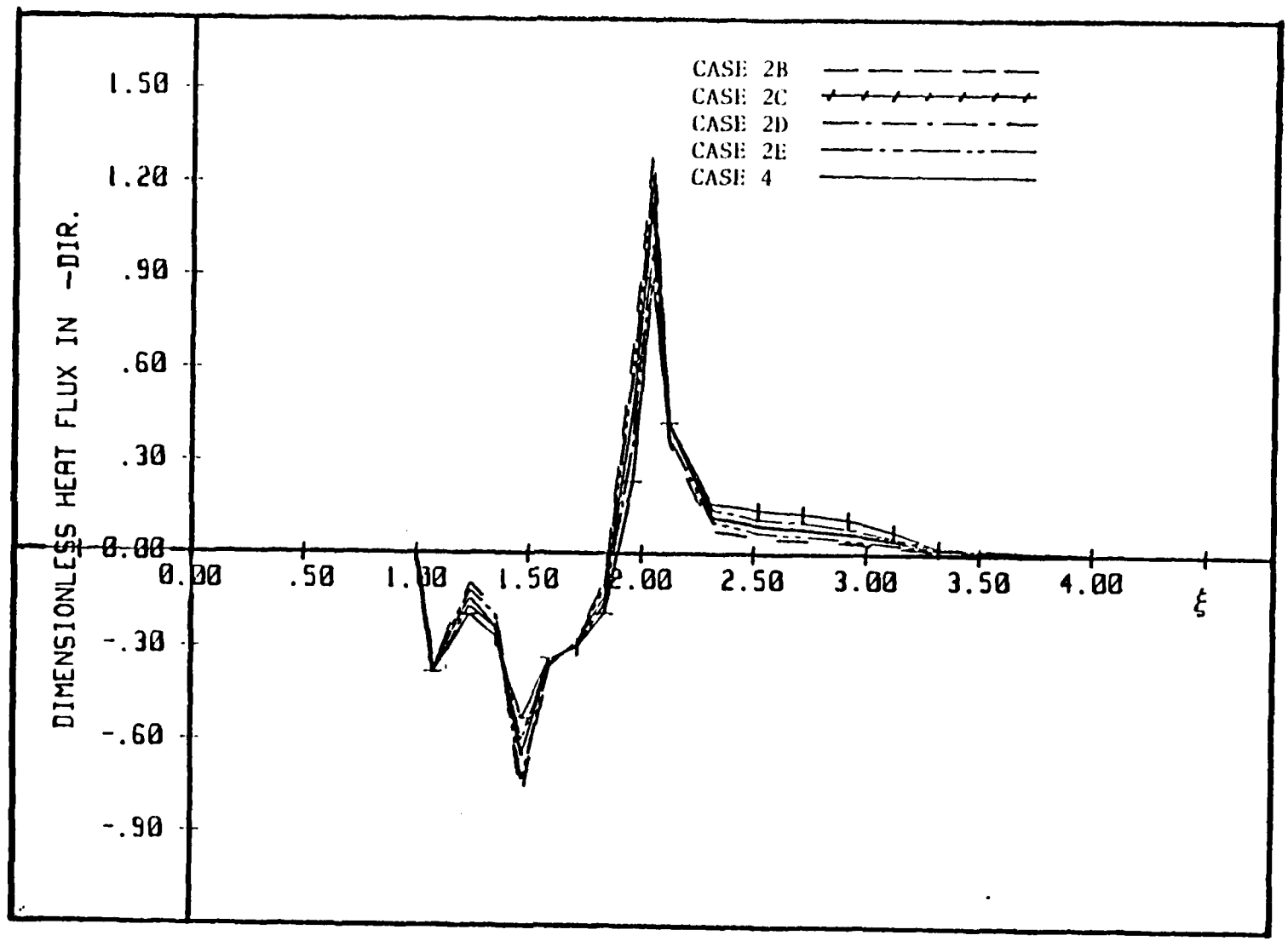

Figure 16. Dimensionless heat flux in ξ-direction, η=0.

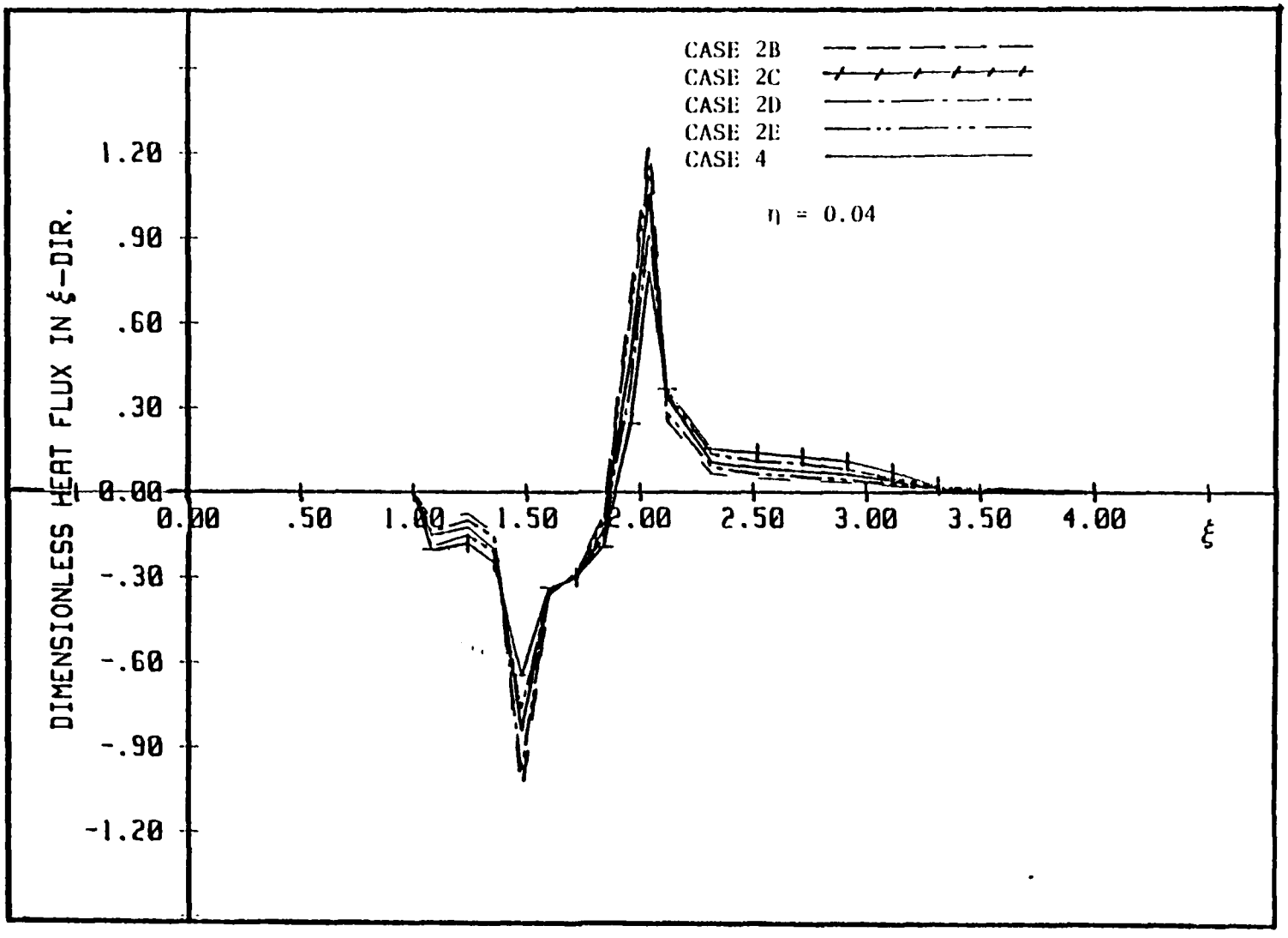

Figure 17. Dimensionless heat flux in ξ-direction, η=0.04.

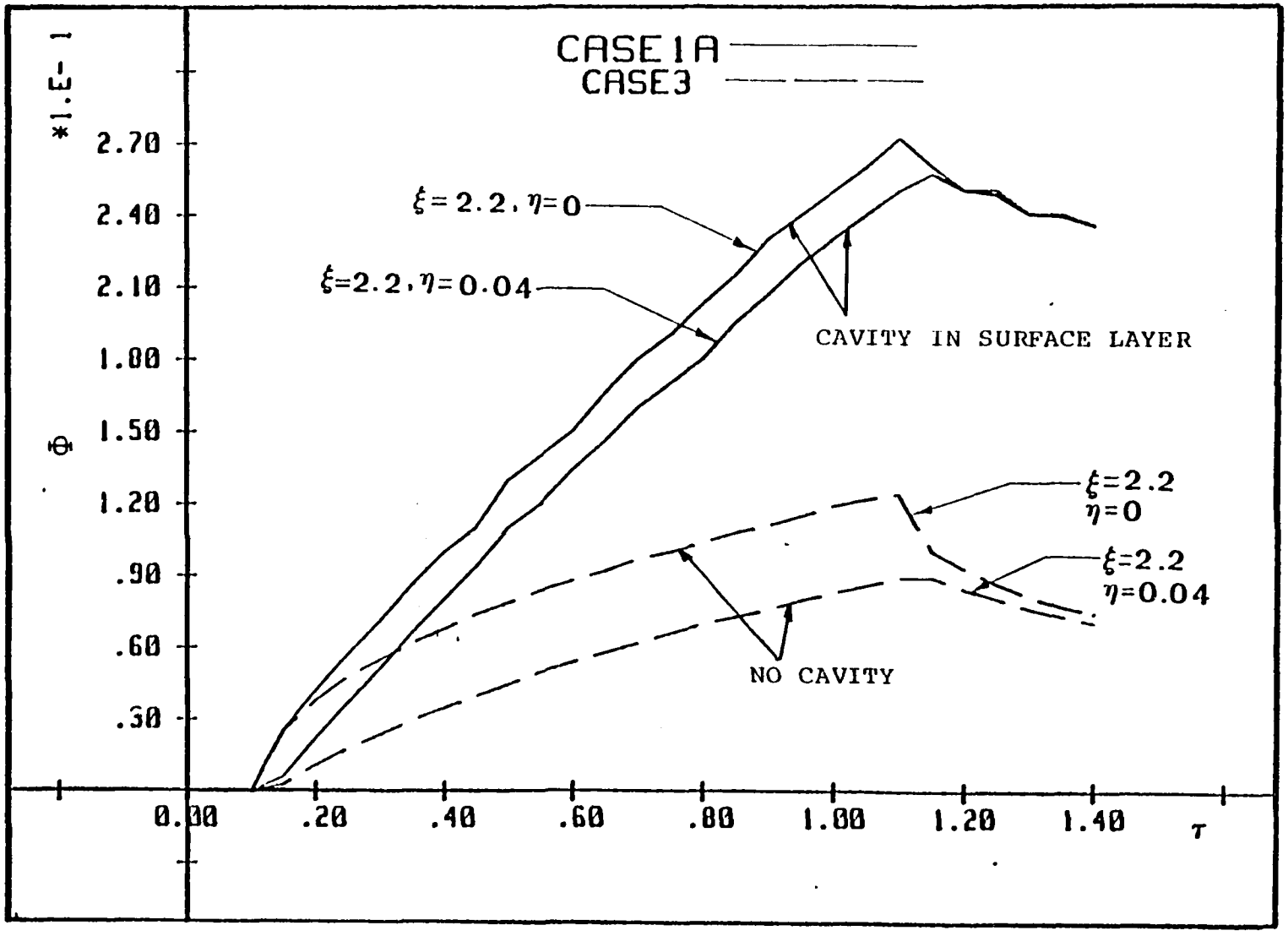

Figure 18. Dimensionless temperature field for single material without cavity and coated material with cavity, L=0.04a.

CHAPTER IV

CONCLUSION

The transient solution to a multiple-boundary problem is always complex. In the current problem, the totality of the boundary is a union of the wear surface, the cavity boundaries, the material interface and infinity. When the transient temperature solution is to be extended in the near future to the transient thermo-mechanical stress solutions, the complexity can only be anticipated. The numerical solution becomes a necessity for analyses in special cases. In the present report, it has been demonstrated that

1. the transient governing differential equations, Equations (1,2), can be formulated into difference equations, Equations (10,11);
2. variable grids (ξ,η), made necessary due to strong local effect, can be transformed into a uniform grid space $(\bar{\xi},\bar{\eta})$;
3. boundary conditions in temperature and/or heat flux can be expressed through energy balance, thus avoiding the problem of singular points such as those of the cavity corners;
4. the numerical solution can be tested by benchmark with a known analytical solution, showing an accuracy of within 1%.

Like most numerical solutions of field problems, functional relationship is not obtainable without volumnous computations. However, significant conclusions can be reached through a few data points.

The numerical variation in the thermal properties of the coating layer confirms the effects of the thermal capacity (ρc) and the thermal conductivity (k), Figure 12, as observed in Huang and Ju [10]. Specifically for

the case when there is a cavity near the wear surface, we can draw the following conclusions:

1. Because of the discontinuity in heat transfer across the void, the temperature will rise higher in the ligament region than the case without the cavity, Figures 9 and 11.
2. The temperature rise is inverse to the ligament volume, Figure 9.
3. When the interface is at the ligament depth, the thermal property of the substrate will influence the temperature gradient, Figure 15.
4. Because of the necessary heat transfer in the lateral direction, the heat flux will be at a large oblique angle to the wear surface. In the case of a layered medium without a cavity the heat flux is in the direction approximately 9° from the perpendicular to the wear surface at a depth of 0.1a. If the coating/substrate interface is in the neighborhood, the resulting delaminating shearing stress is up to 30% of the maximum principal stress, Ju and Liu [2]. With the presence of a cavity, not only the magnitude of the temperature gradient increases, but also the direction of the maximum temperature gradient is rotated to a more oblique angle to the wear surface, Figures 10 and 11. Shear stress in the layer/substrate interface is expected to be huch higher. The temperature field solution thus points to the possibility of a shear delamination between the coating layer and the substrate, because of the presence of a cavity flaw.

REFERENCES

1. Ju, F.D. and Chen, T.Y., "Thermomechanical Cracking in Layered Media from Moving Friction Load," J. of Tribology, Oct. 1984, pp. 513-518.
2. Ju, F.D. and Liu, J.C., "High Speed Asperity Excitation Over a Layered Medium," will be published at Proceeding of International Conference on Advanced Composite Material.
3. Huang, J.H. and Ju, F.D., "Thermomechanical Cracking Due to Moving Friction Load," Part I & II, Wear, Vol. 102, 1985, pp. 81-97.
4. Archard, J.F., "The Temperature of Rubbing Surfaces," Wear, Vol. 2, No. 6, 1959, pp. 438-455.
5. Bannerjee, B.N. and Burton, R.A., "Experimental Studies of Thermoelastic Effects in Hydrodynamically Lubricated Face Seals," J. Lub. Technol., Vol. 101, 1979, pp. 275-282.
6. Ju, F.D. and Huang, J.H., "Heat Checking in the Contact Zone of a Bearing Seal (A Two-Dimensional Model of a Single Moving Asperity)," Wear, Vol. 79, 1982, pp. 107-118.
7. Ling, F.F. and Mow, V.C., "Surface Displacement of a Convective Elastic Half-Space Under an Arbitrary Distributed Fast-Moving Heat Source," J. of Basic Engineering, Sept. 1965, pp. 729-734.
8. Barber, J.R., "Thermoelastic Displacements and Stresses Due to a Heat Source Moving Over the Surface of a Half-Plane," J. of Applied Mechanics, Sept. 1984, Vol. 51, pp. 636-640.
9. Hills, D.A. and Barber, J.R., "Steady Motion of an Insulating Rigid Flat-Ended Punch Over a Thermally Conducting Half-Plane," Thermomechanical Effects in Sliding Systems, Ed. Kennedy, F.E., New York, 1985, pp. 15-22.

10. Huang, J.H. and Ju, F.D., "The Asperity and Material Parameters in Thermomechanical Cracking Due to Moving Friction Load," Proc. Mech. Failures Prevention Group, April 1985 (in print).

11. Ames, W.F., Numerical Methods for Partial Differential Equations, 2nd ed., Academic Press, New York, 1977, pp. 230-311.

12. Forsythe, G.E. and Wascow, W.R., Finite Difference Methods for Partial Differential Equations, John Wiley & Sons, New York, 1960, pp. 88-139.

13. Anderson, D.A., Tannehill, J.C. and Pletcher, R.M., Computational Fluid Mechanics and Heat Transfer, McGraw-Hill Book Company.

14. Karlekar, B.V. and Desmond, R.M., Engineering Heat Transfer, West Publishing Company, New York, 1977, pp. 146-216.

END

5-87

DTIC